공학석사학위논문

Design of the Main Wing in Co-axial Compound Rotorcraft Considering Whirl Flutter Stability

휠 플러터 안정성을 고려한 동축 반전형 복합형 회전익기 주익의 설계 연구

2021년 8월

서울대학교 대학원

협동과정 우주시스템 전공

염 제 완

Design of the Main Wing in Co-axial Compound Rotorcraft Considering Whirl Flutter Stability

지도교수 신 상 준

이 논문을 공학석사 학위논문으로 제출함

2021년 8월

서울대학교 대학원

협동과정 우주시스템전공

염 제 완

염제완의 석사 학위논문을 인준함

2021년 8월

위 원 장 이 관 중

부위원장 신 상 준

위 원 윤 군 진

Abstract

Design of the Main Wing in Co-axial Compound Rotorcraft Considering Whirl Flutter Stability

Jewan Ryeom
Interdisciplinary Program in Space System
The Graduate School
Seoul National University

Rotorcraft has been utilized in various fields thanks to its vertical take-off/landing and hover capability, but is limited in terms of the speed and range due to its aerodynamic aspects such as compressibility, aeroelastic stability, and stall. Recently, there occurs a rise and growth in the research on the compound rotorcraft which has advantages from both fixed and rotary-wing aircraft. Because those have unique configurations distinguished from that of the conventional rotorcraft, new design factors should be taken into account. whirl flutter phenomenon,

which usually occurs in an aircraft with a proprotor, is also observed in the compound rotorcraft with a proprotor, such as the tiltrotor. In this thesis, the three-dimensional feature of the main wing for a compound rotorcraft is suggested. Then three configurations are suggested to find structural integrity variation concerning their composite ply thickness. To estimate its structural intergrity, NASTRAN will be used to perform the relevant static analysis. And, modal analysis is performed and the natural frequencies/eigenvectors will be obtained. With those results, whirl flutter analysis via CAMRAD II and trend analysis using one factor at a time (OAT) method will be performed.

Keywords: Compound Rotorcraft, Main Wing, Structural Analysis, Whirl Flutter Analysis

Student Number: 2019-29018

Contents

List of Tables

List of Figures

Chapter 1

Introduction

1.1 Background and Motivation

Rotorcrafts have played important roles in various fields because of their unique flight capabilities such as vertical take-off/land and hover. Especially Korea has mountainous terrain over its country and the usefulness of vertical flights has been proved in both military and civil sector. Rotorcraft creates lift and thrust through rotating blades, and its flight mechanism causes unique aerodynamic circumstances. When a rotorcraft flies forward, compressibility effects will occur on the rotor blades as shown in Figure 1.1. Forward and inflow speed will be added on the advancing side while will be subtracted in the retreating side causing a stall and reversed flow. Those phenomena not only limit the top speed of rotorcraft but also affect its efficiency as shown in Figure 1.2. In Figure 1.2, the required power of the co-axial configuration at 200kts is similar to the power for hover, while the required power of conventional rotorcraft is at least 50% larger than hovering power. To overcome such weakness, compound rotorcraft which is capable of high forward speed while retaining hover capability

has been developed such as co-axial rotor, tip-jet rotor, tilt-rotor, and so on. Among those various compound rotorcraft, some configurations have proprotors on their wings. Tilt-rotor and co-axial compound rotorcraft are those. In designing these types of compound rotorcraft, whirl flutter should be considered. Lockheed L-188 Electra, a turboprop airliner, suffered two fatal crashes in 1960 due to its whirl-mode flutter. The structure was not strong enough to damp an oscillation and the wings were tore off by excessive oscillation as shown in Figure 1.3. In the compound rotorcraft, the risk of whirl flutter is more dangerous because it has larger rotors, more flexible blades, and gimbal motion compared to a turboprop airliner. Therefore, the whirl flutter has been a major concern in designing compound rotorcraft, especially tiltrotor. To overcome the risk, the wing of the tiltrotor has been designed to be heavier and thicker than the aerodynamically optimal design. Recently, there have been many efforts to predict the whirl flutter stability so the wing feature becomes more efficient while ensuring its safety. Because co-axial compound rotorcraft also has proprotors on its wings, the whirl flutter stability should be considered in this configuration also. In this thesis, the main wing for co-axial compound rotorcraft is designed and whirl flutter analysis is to be presented for various thicknesses of the wing.

1.2 Previous Researches

In this section, the previous research on designing a compound rotorcraft and whirl flutter analysis will be described.

1.2.1 Previous Research about Designing a Compound Rotorcraft

Similar to designing conventional fixed-wing aircraft or rotorcraft, designing compound rotorcraft starts with a conceptual design. This conceptual design usually combines the equations based on the trend line of the existing weight and size database with analyzing skills like the momentum and blade element theory. There have been researches to apply those methods to the compound rotorcraft by modifying the present equations into suitable ones for its unique characteristics. Lee, Jeong, and Yee[3] developed a conceptual design tool for various compound rotorcrafts. Chun et al. performed a design optimization and trade-off study on a fan-in-wing type compound rotorcraft[4]. With the design variables of the diameter of the fan, aspect ratio, taper ratio, sweep angle of both main and tail wing, required power based on the mission profile was calculated by the momentum theory, and weights of each component were calculated by the empirical prediction formulas. As the next step after conceptual design, a preliminary design is the

next phase. In this stage, structural and control analyses are performed and the conceptual design is optimized to fit into the necessary parameters. Yeo and Johnson conducted a design and aeromechanics investigation for a 100,000lb compound rotorcraft[5]. In the paper, Yeo and Johnson analyze the performance, stability, and control considering a condition of 250kts at 4,000ft/95ºF utilizing CAMRAD II. Lim, et al. develop the design optimization tool for compound rotorcraft using CAMRAD II for the aeromechanical analysis and UM/VABS for the cross-sectional analysis[6]. Recently, Hersey, Sridharan, and Celi obtained a rotorcraft preliminary design for a coaxial configuration by a multi-objective design optimization [7].

1.2.2 Previous Research about Whirl flutter Analysis

As mentioned in the previous section, many researches predicting whirl flutter have been conducted recently. Multibody dynamics analysis such as DYMORE and comprehensive rotorcraft analyzing programs such as Comprehensive Analytical Model of Rotorcraft Aerodynamics and Dynamics (CAMRAD) II and Rotorcraft Comprehensive Analysis System (RCAS) are utilized. Also, aeroelastic testbeds such as Wing and Rotor Aeroelastic Test System (WRATS) and TiltRotor Aeroelastic Stability Testbed (TRAST) were constructed for aeroelastic stability

prediction as shown in Figure 1.4. Shen and Kang performed whirl flutter analysis using RCAS and DYMORE[8]. In their paper, they analyzed the WRATS configuration by RCAS and DYMORE. Then the whirl flutter analysis was performed by DYMORE and RCAS and the results were compared with the experimental ones for WRATS. Yeo, et al. developed a tiltrotor analysis by CAMRAD II and RCAS[9]. They started the verification process from the simplest feature including a gimballed rotor, a rigid mast, and rotational springs. Then the complicated feature similar to WRATS was established and verified. Also, they examined the effects on whirl flutter speed in terms of the following parameters: the pitch-flap coupling, blade flexibility, yoke chord, and flap stiffness, pitch link stiffness, rotor rotational speed, atmospheric density, and speed of sound. Yeo and Kreshock performed a whirl flutter study on hingeless proprotors[10]. In the paper, they modeled the tiltrotor installed with hingeless proprotors and examined the effects on whirl flutter speed in terms of the following parameters: the blade flexibility, frequencies, rotor rotational speed, atmospheric density, speed of sound, unsteady aerodynamics, and realistic airfoil tables.

1.3 Research Objectives and Thesis Overview

In Figure 1.5, the overall process of this thesis is presented. First of all, a wing for co-axial compound rotorcraft is designed. The wing consists of skin, D-spar, I-spar, ribs, driveshaft, pylon frame, and pylon skin. Al-7075 T6 is applied for ribs, driveshaft, pylon frame, and pylon skin, composite material is applied for the skin, D-spar, and I-spar. The root area is set to be fixed while the tip area is a free condition like a cantilevered beam. The aerodynamic forces and inertial loads are considered. Three configurations with different design parameters are proposed. Then both static and modal analysis are performed. The static analysis result will be utilized for the structural integrity estimation. And the modal analysis result will be used for the whirl flutter analysis. The eigenvectors and the mode frequencies are obtained by NASTRAN modal analysis and automatically extracted for CAMRAD II by MATLAB. Then whirl flutter stability analysis is performed. In this way, proper design space and parameters can be selected with the results of this study and this will make a good starting point for three-dimensional optimization.

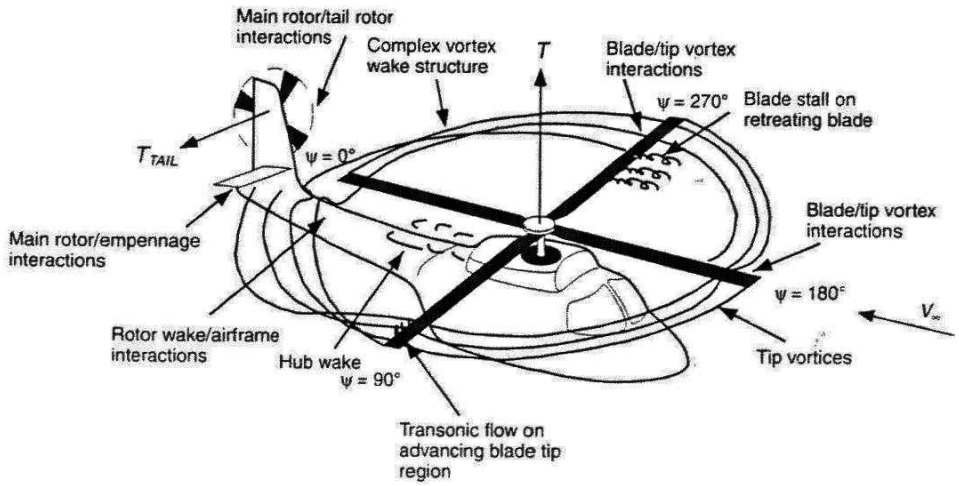

Fig 1.1. Flow field around a rotor disk[1]

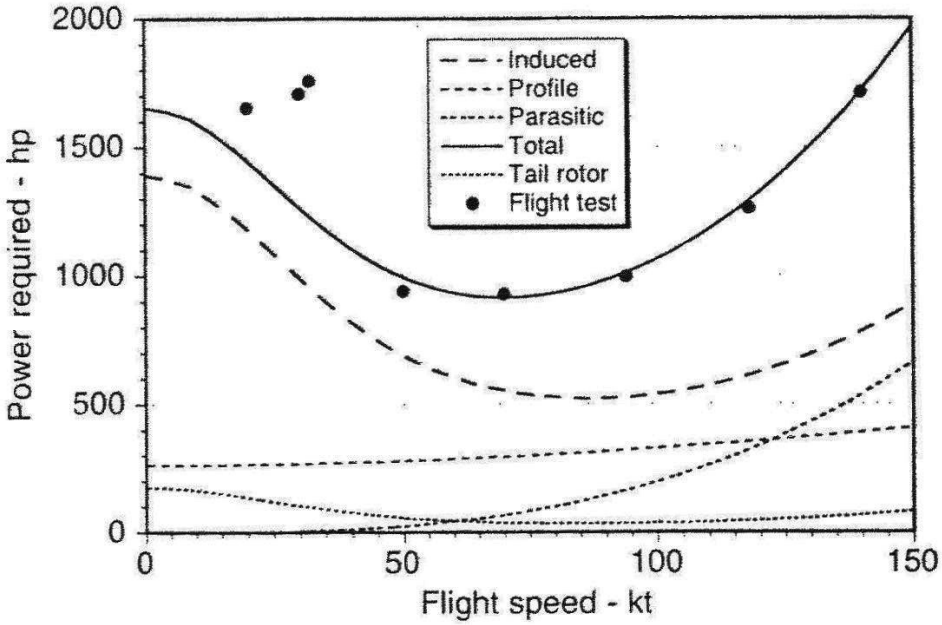

(a) Conventional rotorcraft [1]

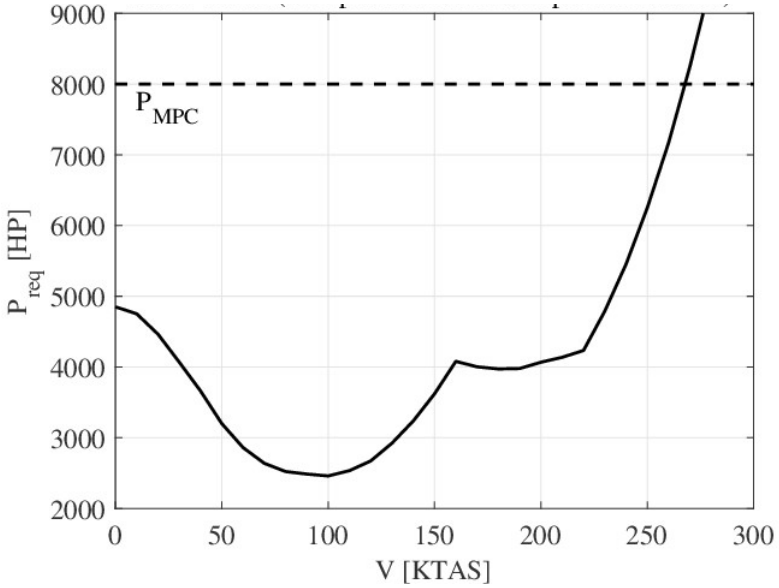

(b) Co-axial configuration [2]

Fig 1.2. Required power versus speed

Fig 1.3. Lockheed L-188 Electra crash due to whirl mode flutter

(a) WRATS

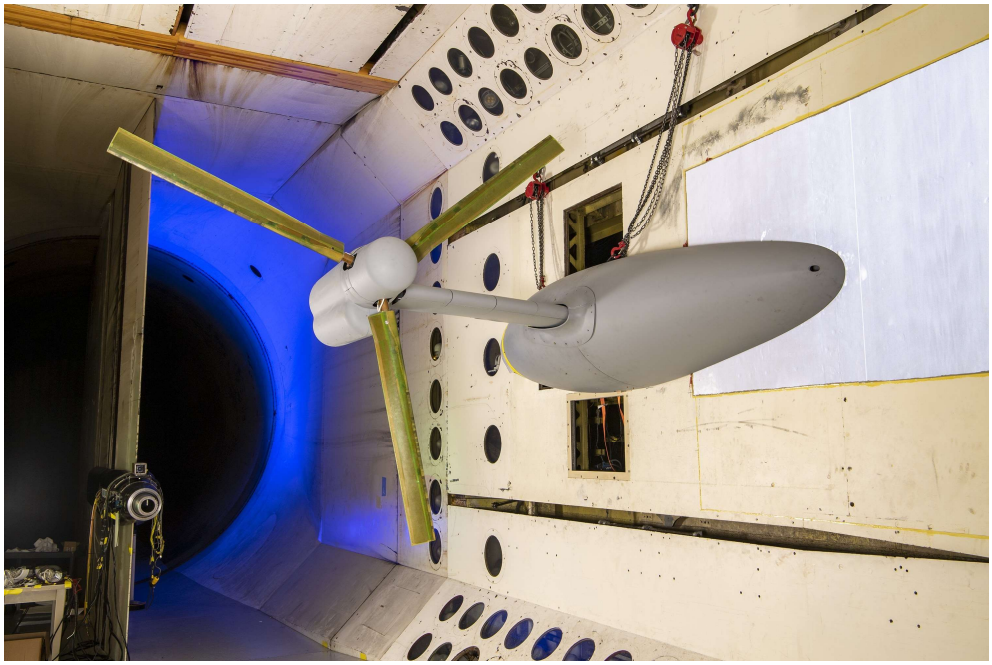

(b) TRAST

Fig 1.4. Aeroelastic stability testbed

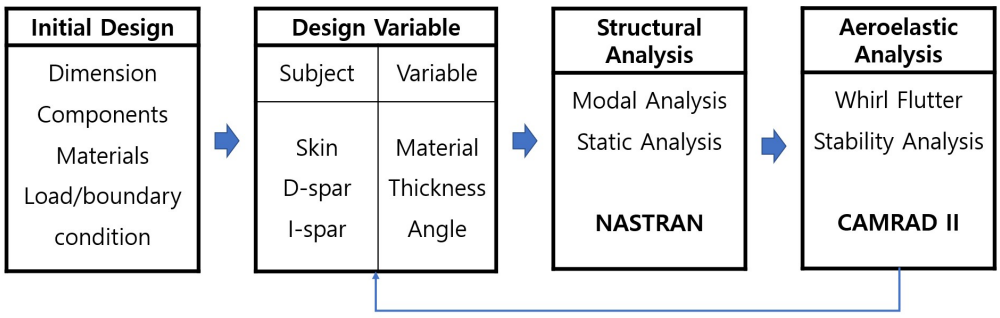

Fig 1.5. Overall process

Chapter 2. Methodology

This chapter introduces the methodology for this thesis. The methodology is explained in the following three parts: structural design, NASTRAN analysis, and whirl flutter analysis.

2.1 Structural Design

In this thesis, the main wing for co-axial compound rotorcraft is designed. The wing is composed of skin, D-spar, I-spar, ribs, driveshaft, pylon skin, and pylon frame. The co-axial compound rotorcraft in this thesis is determined to have a wing and proprotors. The overall wing design is shown in Figure 2.1. The dimensions for the wing are shown in Table 2.1. In this thesis, composite layer and Al7075-T6 are used. Skin, D-spar, I-spar are composed of composite layers. In the composite layers, 3 materials are utilized: CF3327, Carbon UD, GF108. Other components including ribs, driveshaft, pylon skin, and pylon frame are made with Al-7075 T6. Those material properties are shown in Table 2.2. and 2.3. Unlike most of the tiltrotors, this co-axial compound rotorcraft has its engine under the main rotor and the power for proprotors is transmitted via a drive shaft. Thus the pylon is considered to carry a propeller and transmission without an engine. To decide the

dimension of the drive shaft, the following equations for torque transmission and torsional buckling capacity are utilized.

Torque transmission capacity:

$$T = 2 \times \pi \times r^2 \times t \times S_S \tag{2-1}$$

Torsional buckling capacity for a long shaft:

$$\tau_{cr} = \frac{E}{3\sqrt{2}(1-\nu^2)^{\frac{3}{4}}}(\frac{t}{r})^{\frac{3}{2}} \tag{2-2}$$

r: mean radius, t: thickness, S_S: shear strength, ν: Poisson's ratio, E: elastic modulus

The safety factor is determined to be 2.5 which is commonly used in the literature range[11]. Considering the safety margin and the transmitted torque, the shaft is decided to have an outer radius of 0.03m and thickness of 0.003m. The bearings for the driveshaft are considered to be in the ribs and their weight is set to be 0.1kg for each bearing by the data from commercial products. There are 2 types of spars for the wing: D-spar and I spar. The locations of the spars are decided with a reference to Endres[12]. 9 ribs are considered and their thickness is decided to be 0.003m with a reference to Dharmendra[13].

2.2 NASTRAN Analysis

In this thesis, NASTRAN is utilized to perform the relevant static and modal analysis. The discretized feature of the wing is created with the shell and solid elements in NASTRAN based on the three-dimensional drawing as shown in Figure 2.2. As the boundary condition, the root of the wing is fixed while the tip is in a free state. Considering the aerodynamic forces, the C81 table for NACA 23012 is looked up. Lift, drag, and aerodynamic pitching moment are applied to the elements based on the table. The weight of the propeller and the transmission are considered on the pylon frame as CONM2 elements. The gravitational acceleration is applied as an inertial load. Proper contact condition is applied on each component as shown in Table 2.4. After performing the static analysis, the maximum stress in each layer is predicted. With the strength in each direction shown in Table 2.2, the safety margin will be obtained. The safety factor is 2 based on the Federal Aviation Regulation Sec. 25.303. Then the eigenvectors and mode frequencies are obtained through the modal analysis. By MATLAB, those values are automatically extracted from the f06 file of NASTRAN result files and saved as parameters for CAMRAD II whirl flutter stability analysis.

2.3 Whirl Flutter Analysis

2.3.1. Whirl Flutter

Whirl flutter instability is an aeroelastic flutter instability that may appear on the aircraft with a propeller on its wing. It occurs because of the dynamic and aerodynamic effects of rotating parts, such as a rotor or a propeller. The rotating mass generates additional forces and moments and increases the number of degrees of freedom. Also, an aerodynamic interference effect between a propeller and a wing is created by rotating propellers. Whirl flutter instability is driven by unsteady aerodynamic propeller forces and moments acting on the propeller plane. It causes unstable vibration leading to a crash.

To describe the principle of the whirl flutter phenomenon, a simple mechanical system with two degrees of freedom is assumed. The propeller and hub are considered to be rigid. Two rotational springs which have stiffnesses of K_Ψ, K_Θ are applied to describe a flexible engine mounting as illustrated in Figure 2.3. There are two independent mode shapes of yaw and pitch as shown in Figure 2.4. The gyroscopic motion causes the change of the angles of attack of the propeller blades. This change causes unsteady aerodynamic forces which may induce whirl flutter instability. The most important terms regarding whirl flutter are yaw moment and pitch moment. These moments are to

be balanced by aerodynamic or structural damping terms and the state of neutral stability with no damping represents the flutter state. The airflow speed at this moment is called the critical flutter speed. The stable and unstable states of the gyroscopic system are applicable in terms of flutter. Both states are described in Figure 2.5. Unless the air velocity is smaller than the critical flutter speed, the gyroscopic motion will be damped and the aircraft will be stable. But the airspeed over the critical flutter speed causes the instability of the system with the divergence of the gyroscopic motion.

2.3.2. Whirl Flutter Analysis Model

CAMRAD II whirl flutter analysis estimates the interaction between the rotor and wing frame modes. The present CAMRAD II input configuration is as shown in Figure 2.6. 7 nonlinear beam elements and 15 aerodynamic panels are used. Uniform inflow model based on the momentum theory and zero torque trim for a pusher propeller is assumed to represent the severest condition. To consider the aerodynamic forces and moments of the wing, C81 table for NACA 23102 is looked up. Because the propeller nacelle is assumed to be installed at the tip of the wing, the wing wake effect and the aerodynamic interaction between the rotor and wing are assumed to

have little effects are ignored[15]. The wing mode information(eigenvectors, mode frequencies) from NASTRAN and the information of the wing airframe, the wing feature, the rotor feature, and the rotor properties are used as input. The structural damping is set to be 1.0% as Yeo applied on his configuration[15]. To consider δ_3 angle, equivalent pitch bearing is modeled by the following equations.

$$\epsilon = L_{ph}\tan\theta \approx L_{ph}\theta \tag{2-3}$$

$$F = K_{pl}\epsilon = \frac{EA_{pl}}{L_{pl}}\epsilon = \frac{EA_{pl}}{L_{pl}}L_{ph}\theta \tag{2-4}$$

$$M = FL_{ph}\sin\alpha = \frac{EA_{pl}}{L_{pl}}L_{ph}^2\sin\alpha\theta = k_\theta\theta \tag{2-5}$$

$$k_\theta = \frac{EA_{pl}}{L_{pl}}L_{ph}^2\sin\alpha \tag{2-6}$$

$$epitch = L_{ph}\sin\alpha\tan\delta_3 + L_{ph}\cos\alpha \tag{2-7}$$

Symbols used in the equations such as ϵ, α, δ_3 can be found in Figure 2.7. In this thesis, δ_3 is set to be –45º to represent the severest condition. CAMRAD II input file is verified with the XV-15 baseline configuration. For the wing mode information, NASTRAN detailed FEM results are utilized. δ_3 is －15° and the relevant whirl flutter stability analysis results are shown in Figure 2.8. As shown in Figure 2.8, the predicted whirl flutter speed is 30kts lower than the result of XV-15.

But the frequencies are almost the same and the tendency is well matched. Thus, the overall analysis capability is verified. The whirl flutter analysis on XV-15 is also presented in Acree, et al.[16] In that analysis, the wing chord mode was shown to be a major factor of whirl flutter and the whirl flutter speed was obtained to be 275kts. However, the whirl flutter speed for the thick wing configuration was found to be about 330kts which signified the change of wing thickness may affect whirl flutter speed.

2.4 Design Configurations

In this thesis, three design configurations will be examined. Since the thickness is an important factor for both static stability and whirl flutter stability, the thickness of each composite layer is varied along with the design configurations as shown in Table 2.5. From those configurations, the tendency of stress level and whirl flutter speed will be studied in terms of the wing thickness.

2.5 Analysis on the Critical Damping

After the analyses on the three design configurations are completed,

the trend analysis for critical modal damping and weight will be performed. Critical damping is an important factor related to the whirl flutter phenomenon. Wing stiffness is an important factor since the whirl flutter occurs by the interaction between the wing and rotor vibration. Therefore, this analysis will be performed to evaluate the impact of the wing stiffness by intentionally changing its parameters. One factor at a time (OAT) method is utilized. As shown in Table 2.6, the baseline configuration is the same as Configuration 1 used before. Then 8 configurations varying with the thickness of each layer except GF108 will be generated. The results will be compared with the baseline whirl flutter stability analysis result. From those configurations, the tendency of the critical damping will be studied.

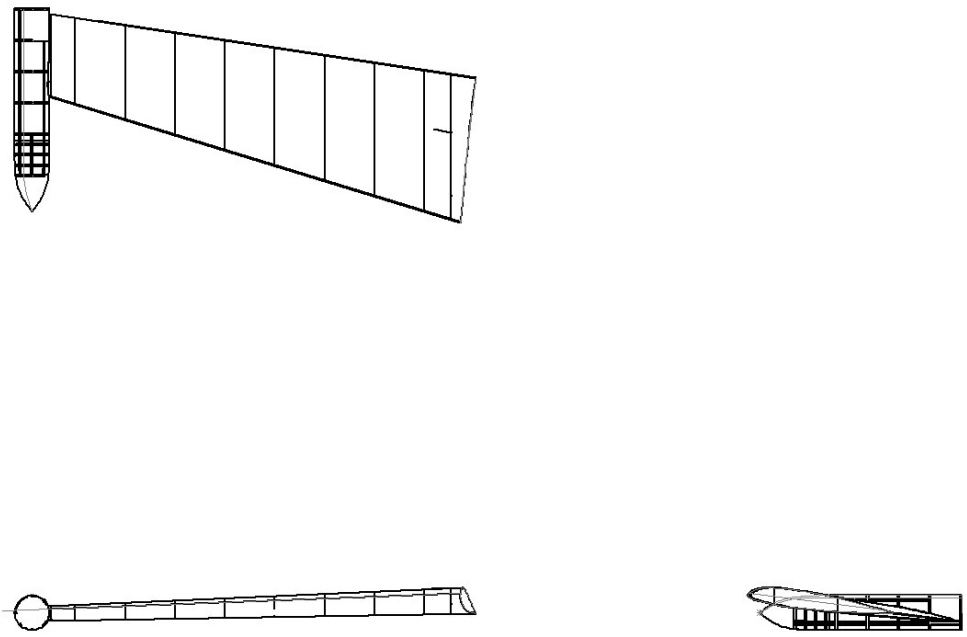

Fig 2.1 Three-dimensional wing design

Table 2.1 Geometry information

Aspect ratio	9
Taper ratio	0.5
Chord length (root)	2.7
Chord length (tip)	1.4
Wing span (ft)	18
Wing sweep (°)	14.9
Incidence angle (°)	6.9

Table 2.2 Composite material properties

Type	CF3327	Carbon UD	GF108
E_{11} (Pa)	4.74×10^{10}	1.00×10^{11}	2.13×10^{10}
E_{22} (Pa)	5.20×10^{10}	4.21×10^{9}	2.02×10^{10}
E_{33} (Pa)	5.20×10^{10}	4.21×10^{9}	2.02×10^{10}
G_{12} (Pa)	5.03×10^{9}	5.86×10^{9}	3.73×10^{9}
G_{23} (Pa)	2.00×10^{10}	1.62×10^{9}	7.78×10^{9}
G_{31} (Pa)	2.00×10^{10}	1.62×10^{9}	8.18×10^{9}
ν_{12}	0.055	0.312	0.147
ν_{23}	0.3	0.3	0.3
ν_{31}	0.3	0.3	0.3
Density (kg/m^3)	1,443	1,751	1520
$Allowable\ stress_{11}$ (Pa)	3.50×10^{9}	1.46×10^{10}	2.03×10^{9}
$Allowable\ stress_{22}$ (Pa)	3.12×10^{9}	1.60×10^{8}	1.96×10^{9}
$Allowable\ stress_{12}$ (Pa)	4.30×10^{8}	2.00×10^{8}	3.00×10^{8}
$Allowable\ strain_{11}$ ($\mu\epsilon$)	7,000	17,000	12,000
$Allowable\ strain_{22}$ ($\mu\epsilon$)	6,000	3,000	11,000
$Allowable\ strain_{12}$ ($\mu\epsilon$)	11,000	5,000	10,000

Table 2.3 Al7075-T6 properties

Type	
E_{11} (Pa)	7.17×10^{10}
E_{22} (Pa)	7.17×10^{10}
E_{33} (Pa)	7.17×10^{10}
G_{12} (Pa)	2.69×10^{10}
G_{23} (Pa)	2.69×10^{10}
G_{31} (Pa)	2.69×10^{10}
ν_{12}	0.33
ν_{23}	0.33
ν_{31}	0.33
Density (kg/m^3)	2,810
$Allowable\ stress_{11}$ (Pa)	5.03×10^{8}
$Allowable\ stress_{22}$ (Pa)	5.03×10^{8}
$Allowable\ stress_{12}$ (Pa)	3.31×10^{8}
$Allowable\ strain_{11}$ ($\mu\epsilon$)	110,000
$Allowable\ strain_{22}$ ($\mu\epsilon$)	110,000
$Allowable\ strain_{12}$ ($\mu\epsilon$)	110,000

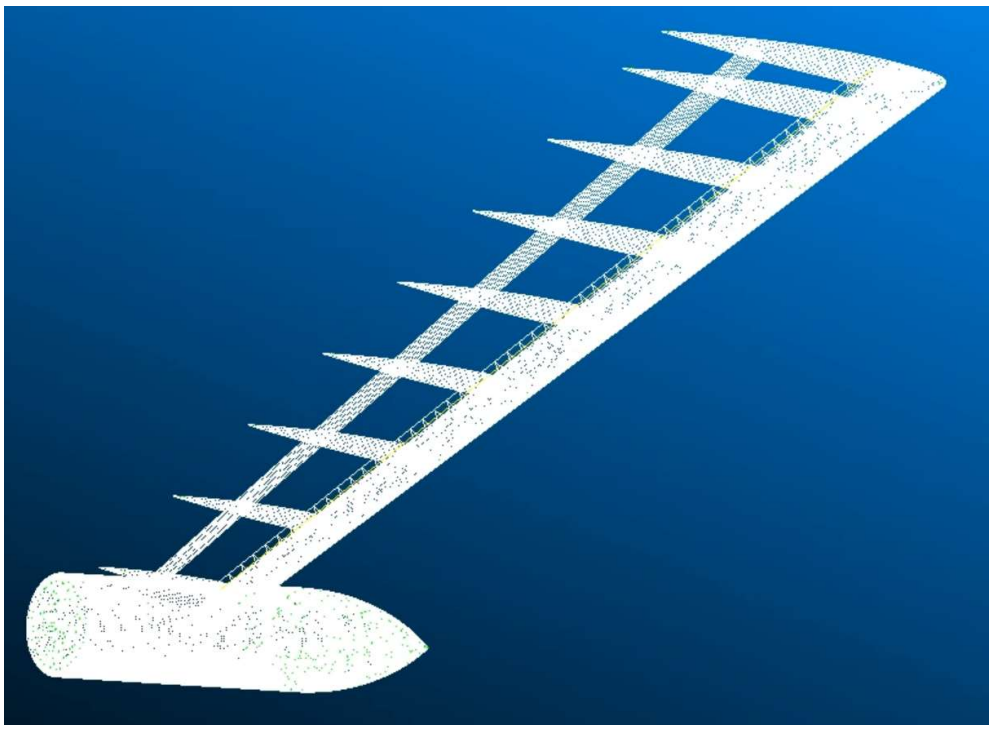

Fig 2.2 Discretized configuration of the wing in NASTRAN

Table 2.4 Contact information

	D-spar	Pylon frame	Pylon skin	Ribs	Drive shaft	Skin	I-spar
D-spar		Glued		Glued		Glued	
Pylon frame	Glued		Glued				Glued
Pylon skin		Glued				Glued	
Ribs	Glued				Glued	Glued	Glued
Drive shaft				Glued			
Skin	Glued		Glued	Glued			Glued
I-spar		Glued		Glued		Glued	

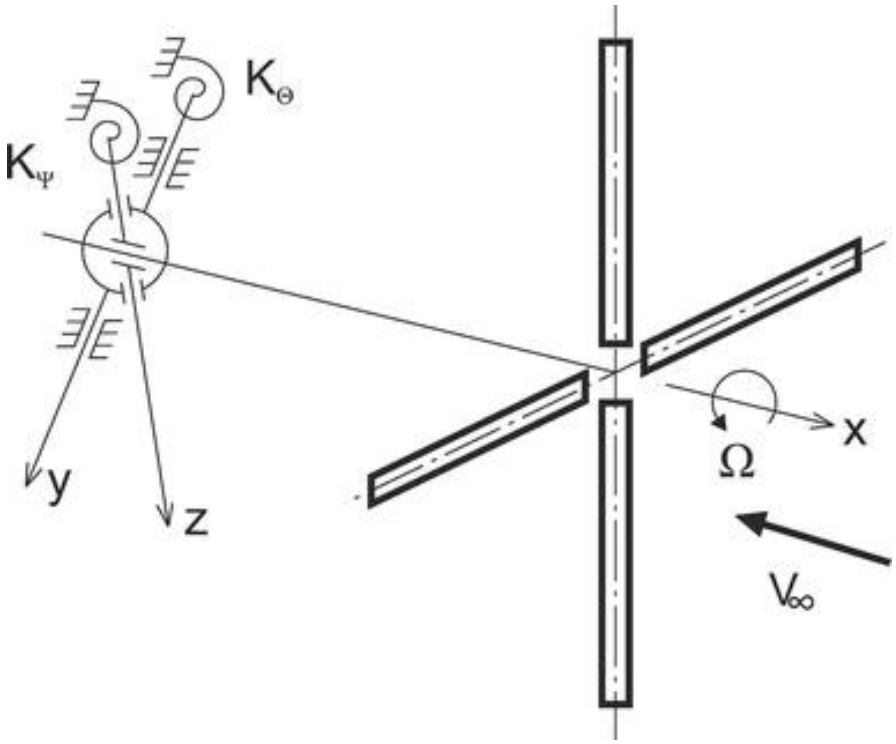

Fig 2.3 Two-degree-of-freedom system with a propeller[14]

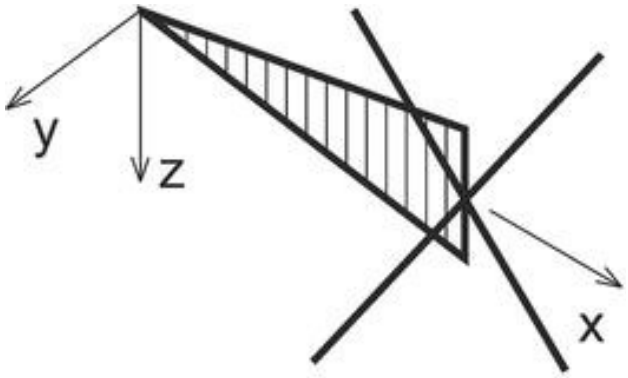

(a) Pitch

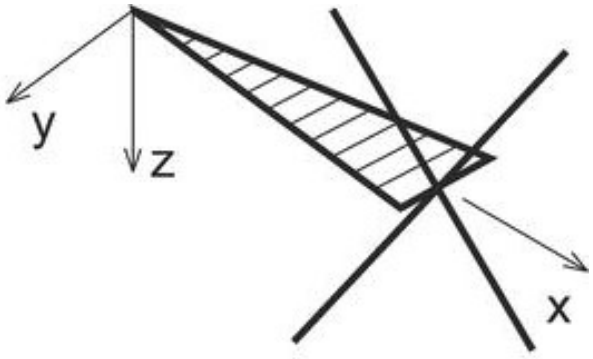

(b) Yaw

Fig 2.4 Independent mode shapes[14]

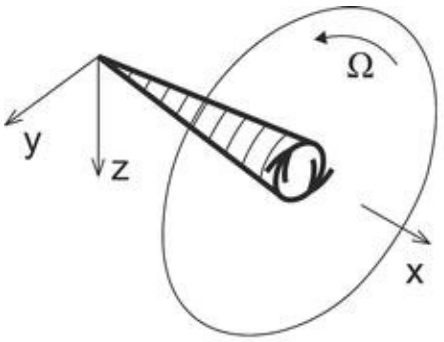

(a) Backward whirl modes

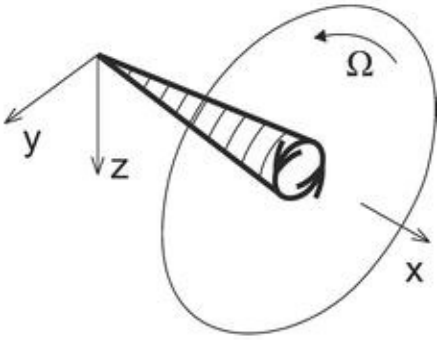

(b) Forward whirl modes

Fig 2.5 whirl modes[14]

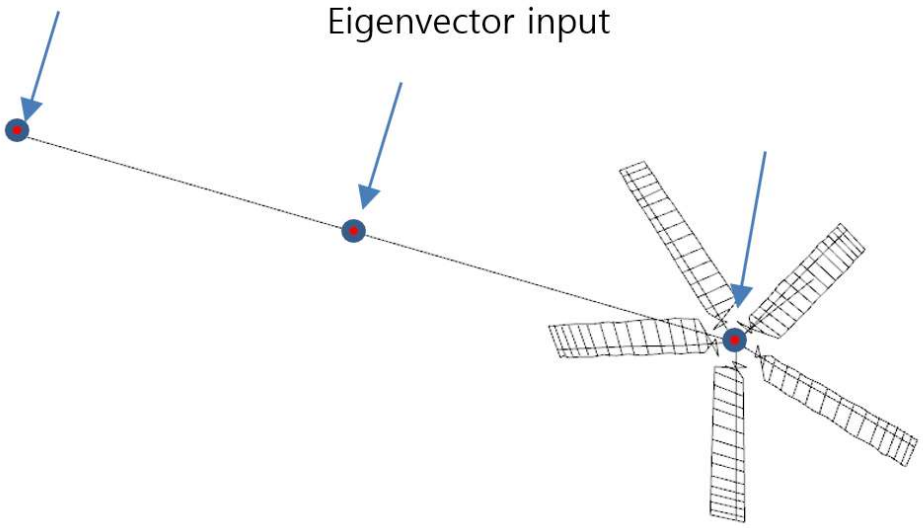

Fig 2.6 CAMRAD input configuration for the whirl flutter analysis

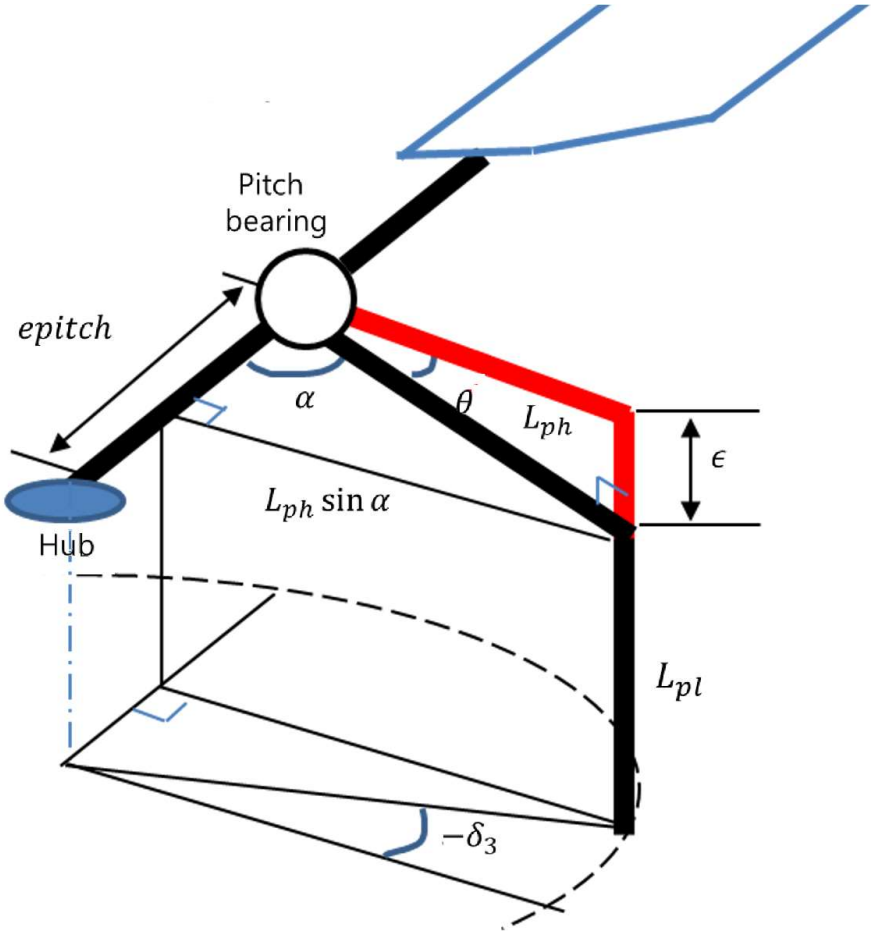

Fig 2.7 Equivalent pitch bearing

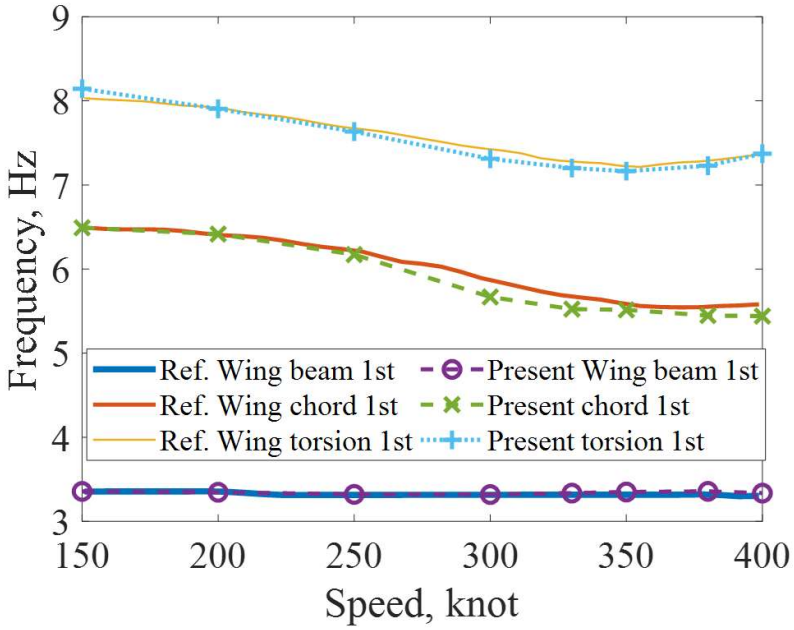

(a) Frequency vs Speed

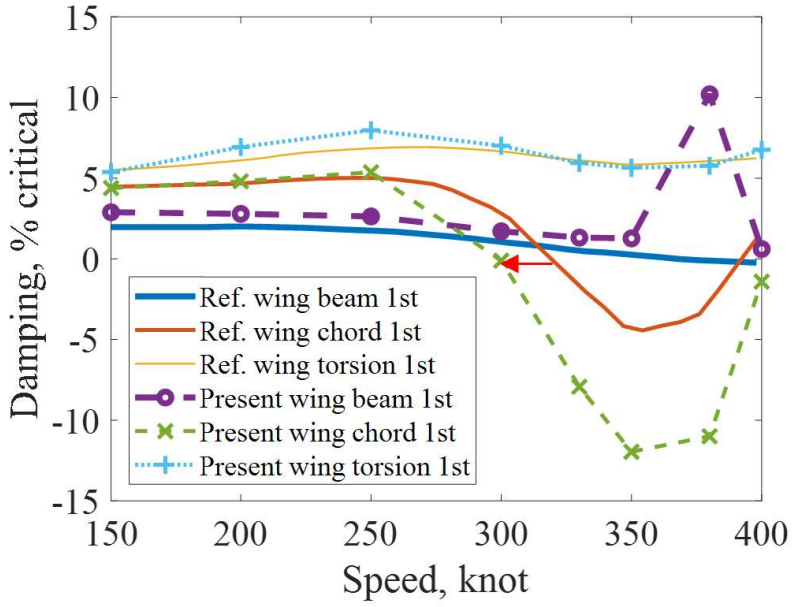

(b) Damping vs Speed

Fig 2.8 XV-15 whirl flutter analysis result

Table 2.5 Design configurations

		Configuration 1	Configuration 2	Configuration 3
Skin (mm)	GF108	0.1	0.1	0.1
	CF3327 0º	0.54	0.27	0.27
	CF3327 45º	0.54	0.27	0
	Carbon UD	0.6	0.3	0.3
D-spar (mm)	GF108	0.1	0.1	0.1
	CF3327 0º	0.54	0.27	0.27
	CF3327 45º	0.54	0.27	0
I-spar (mm)	GF108	0.1	0.1	0.1
	CF3327 0º	0.54	0.27	0.27
	CF3327 45º	0.54	0.27	0
	Carbon UD	0.6	0.3	0.3

Table 2.6 Thickness information

		Baseline Thickness	Thickness per a layer	Corresponding configuration
Skin (mm)	GF108	0.1	0.1	-
	CF3327 0º	0.54	0.27	Configuration 4
	CF3327 45º	0.54	0.27	Configuration 5
	Carbon UD	0.6	0.3	Configuration 6
D-spar (mm)	GF108	0.1	0.1	-
	CF3327 0º	0.54	0.27	Configuration 7
	CF3327 45º	0.54	0.27	Configuration 8
I-spar (mm)	GF108	0.1	0.1	-
	CF3327 0º	0.54	0.27	Configuration 9
	CF3327 45º	0.54	0.27	Configuration 10
	Carbon UD	0.6	0.3	Configuration 11

Chapter 3. Numerical Results

In this chapter, the analysis results will be described. First, the static analysis results will be shown. Then the modal analyses are performed and the whirl flutter analysis results will be presented. Finally, the trend analysis results will be displayed.

3.1 Static Analysis Results

As mentioned in the previous chapter, the static analysis under 250kts cruise flight condition is performed by using NASTRAN. As shown in Figure 3.1, the maximum stress over allowable stress is found in the Carbon UD layer of I spar for Configuration 1. It is found to be 8.2% in shear direction, and thus the structure has much margin to become light. Because the shear strength of the Carbon UD layer is small, usually the maximum stress over allowable stress is found in the Carbon UD layer. But in D spar, CF3327 layer in longitudinal direction shows the maximum stress over allowable stress in the component. As shown in Figure 3.2, the maximum stress over allowable stress is found in the UD layer of skin for Configuration 2. The maximum stress is found in shear direction and almost 11.1% of its allowable stress. The layer and direction of maximums stress in each component are the

same as in the previous configuration. In Configuration 3, the maximum stress over allowable stress reaches up to 51.5% as shown in Figure 3.3. This occurs in the UD layer of the I-spar, shear direction. The maximum stress over allowable stress in the other components are over 10%. In D spar, CF3327 layer in the longitudinal direction shows 11.4%. Carbon UD layer of skin in shear direction has the maximum stress of 17.1% of its allowable stress. While the stress level increases dramatically, there will be about 1kg of change in the mass between Configuration 2 and 3 as shown in Figure 3.4. Hence, Configuration 3 may become the lower limit of the design space for the future optimization processes.

3.2 Modal Analysis Results

After the static analysis is completed, the modal analysis will be performed. There are two important outputs from modal analysis. One is the mode frequency and the other is the eigenvector. Figures 3.5 to 3.7 shows the modal analysis results of Configurations 1 to 3. All of the configurations show the 1^{st} beam mode, 1^{st} chord-torsion mode, 1^{st} torsion mode, and 2^{nd} beam mode. But in Configuration 3, the 1^{st} torsion mode frequency is smaller than that of the 1^{st} chord-torsion mode. As shown in Figure 3.8, the frequencies of each mode become

smaller as the wing thickness becomes thinner. To perform the whirl flutter analysis, the eigenvectors from the minimum of 3 nodes are required. Therefore, there are 3 nodes selected. The 1st node is at the tip, the 2nd node is at the center and the 3rd node is at the root. All of the nodes are 0.25c in the chordwise direction. The rotor frequencies are estimated by CAMRAD and shown to be 86.4Hz for the prop flap 1st mode and 103.5Hz for the prop torsion 1st mode.

3.3 Whirl Flutter Analysis Results

With the eigenvectors and mode frequencies from NASTRAN modal analysis, the whirl flutter analysis is performed. As shown in Figures 3.9 to 3.13, the critical damping value has the smallest value around 200kts with the wing chord-torsion 1st mode. But all of their damping values are shown to be positive in the entire examination region. The minimum critical damping values are presented in Table 3.2. Even though changing the thickness of the same material in the same component, it is shown to have different minimum critical damping values in accordance with the orientation angle of the ply. Therefore, not only the material and location but also the angle of the composite ply affects the critical damping value. Because the mode frequency and the mode eigenvectors are changed along with those parameters, the

whirl flutter speed is affected. Further investigation on the impact of those parameters is performed in the trend analysis.

3.4 Trend Analysis Result

As previously shown, the critical damping values change with respect to the wing stiffness. To examine the impact of the design parameters, trend analysis will be performed. In the trend analysis, the minimum critical damping value and weight of each configuration are compared with those of the baseline. The flutter analysis results are presented in Figures 3.14 to 3.21. As shown in Figure 3.22, the critical damping reduces in the skin CF3327 0° most while the I-spar CF3327 45° shows the least change. The critical damping reduction affects the whirl flutter instability, and thus the less damping reduction is better for the stable flight. The weight reduction in Figure 3.23 shows the biggest value in the skin Carbon-UD layer, while the I-spar CF3327 layer shows the least change. It is shown that if the thickness of one of the layer should be reduced, the skin CF3327 45°, D-spar 0°, and I-spar CF3327 45° is a better option than their different orientation angle counterparts. These results can be utilized to built proper design space for optimization in future researches.

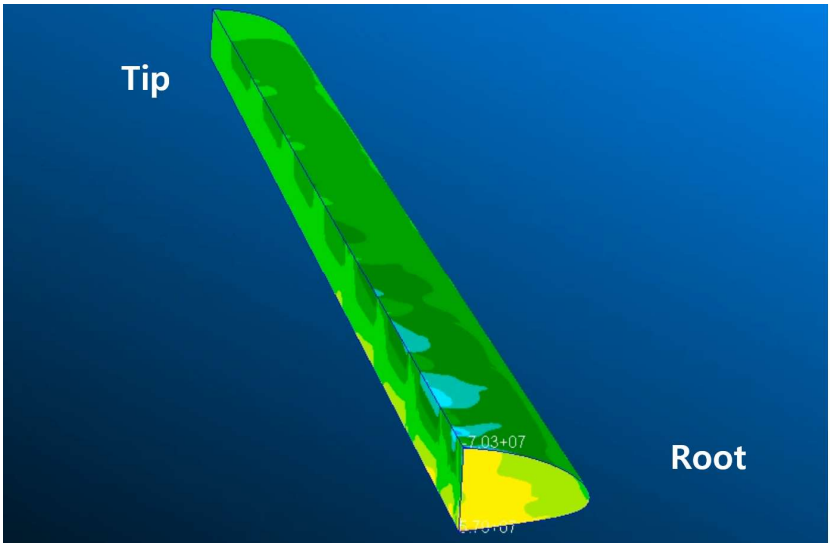

(a) D-spar, CF layer, longitudinal

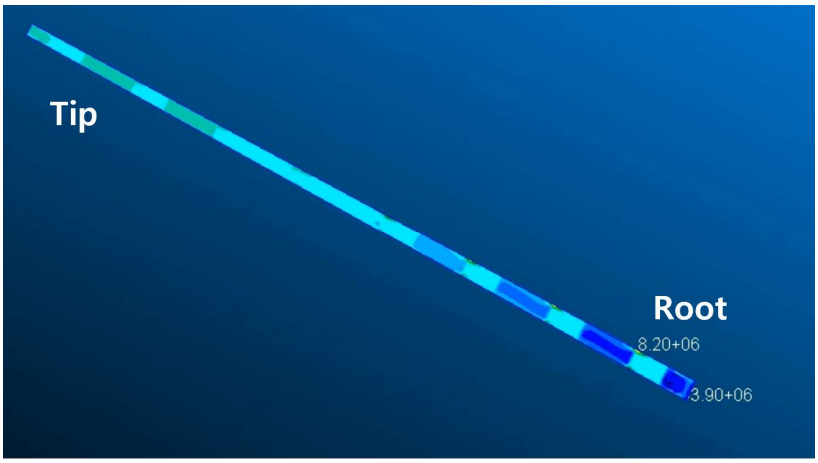

(b) I-spar, UD layer, shear

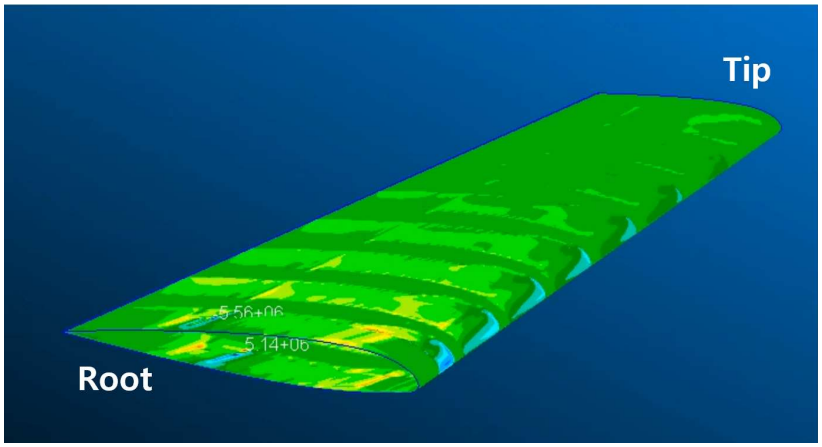

(c) Skin, UD layer, shear

Fig 3.1 Maximum stress layers in each component of Configuration 1

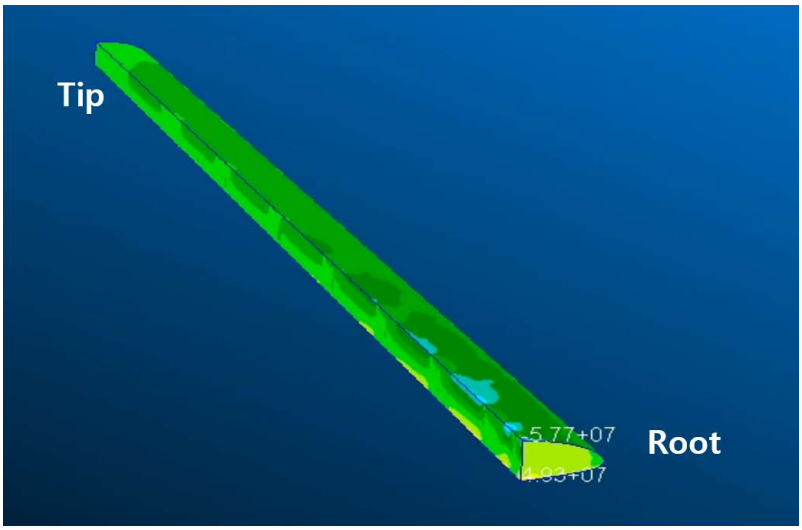

(a) D-spar, CF layer, longitudinal

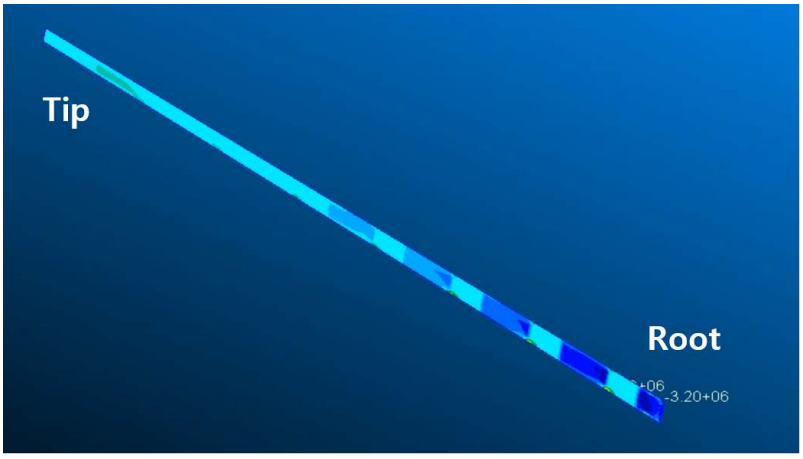

(b) I-spar, UD layer, shear

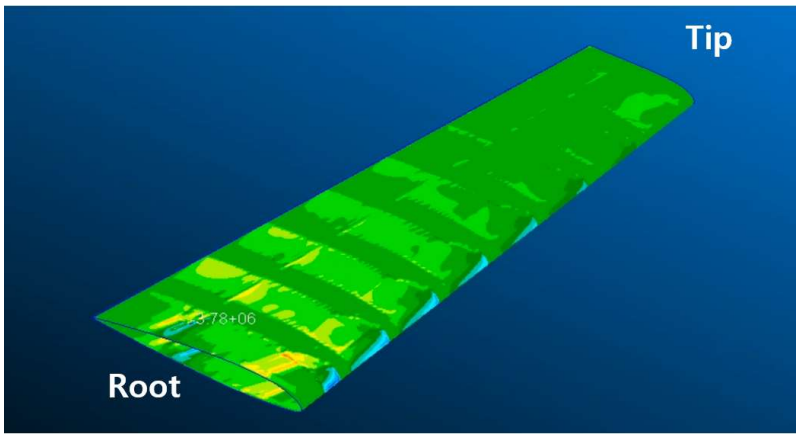

(c) Skin, UD layer, shear

Fig 3.2 Maximum stress layers in each component of Configuration 2

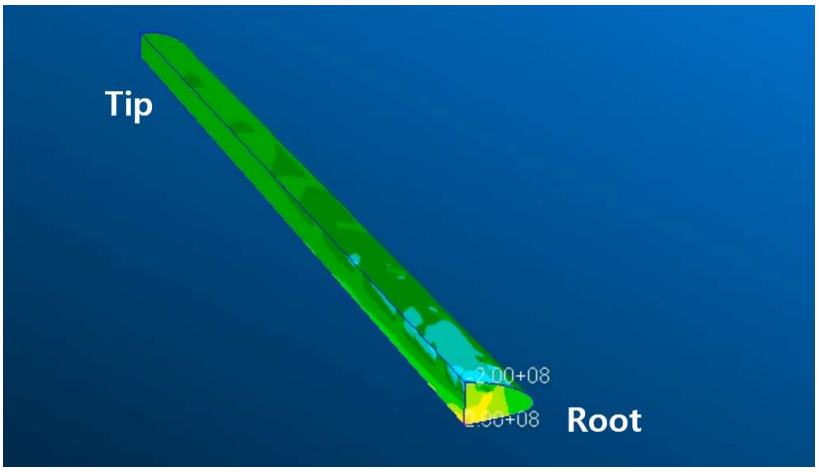

(a) D-spar, CF layer, longitudinal

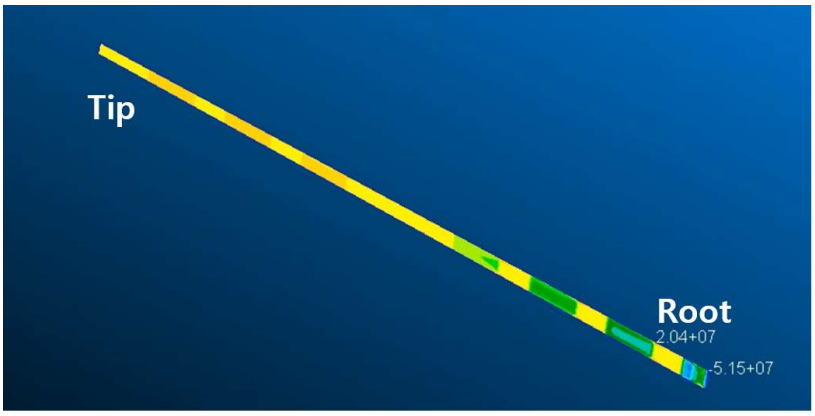

(b) I-spar, UD layer, shear

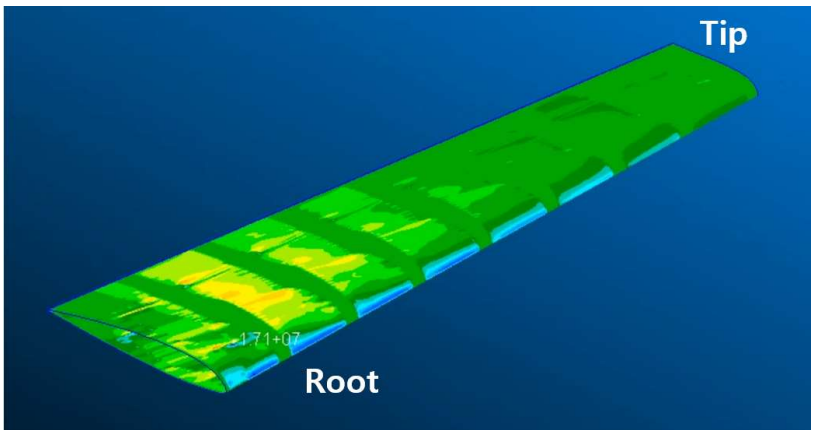

(c) Skin, UD layer, shear

Fig 3.3 Maximum stress layers in each component of Configuration 3

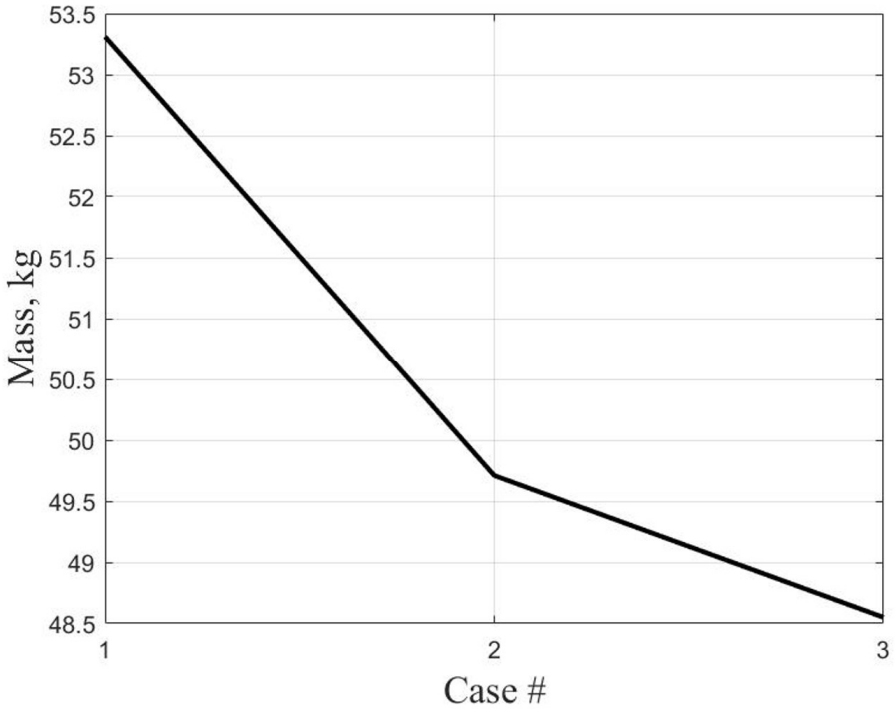

(a) Mass of each configuration

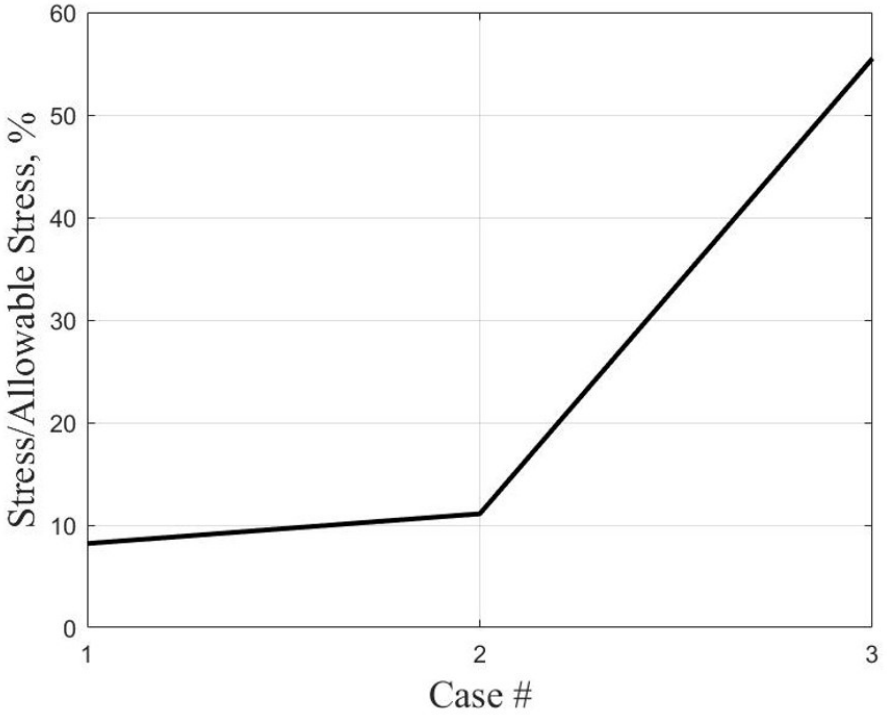

(b) Maximum stress/allowable stress of each configuration

Fig 3.4 Static analysis result comparison

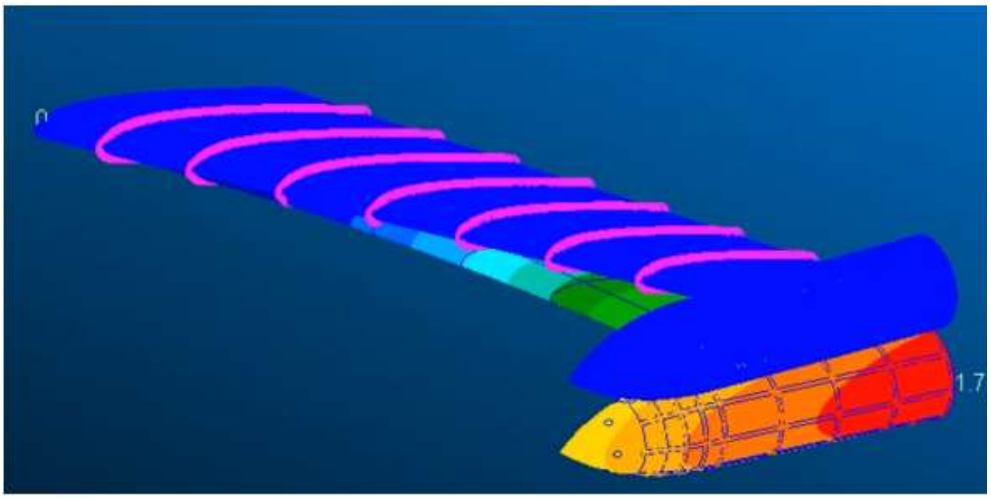

(a) Beam 1st mode 7.48Hz

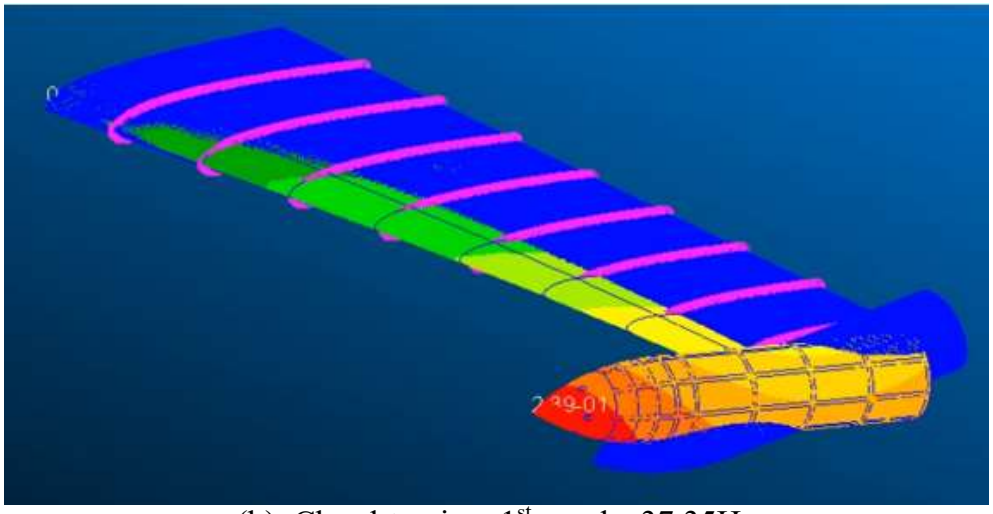

(b) Chord-torsion 1st mode 37.35Hz

Fig 3.5 Modal analysis result of Configuration 1 (contd.)

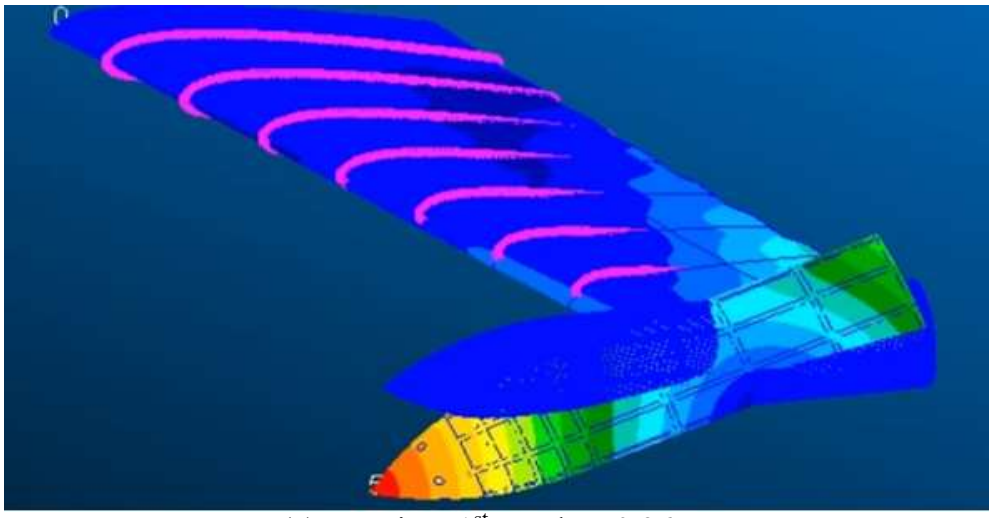

(c) Torsion 1st mode 50.96Hz

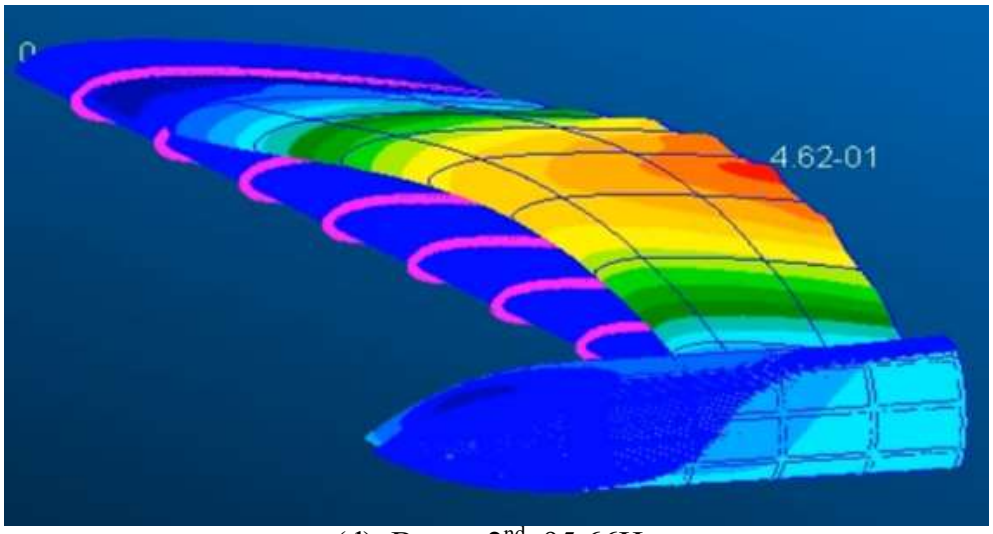

(d) Beam 2nd 95.66Hz

Fig 3.5 Modal analysis result of Configuration 1

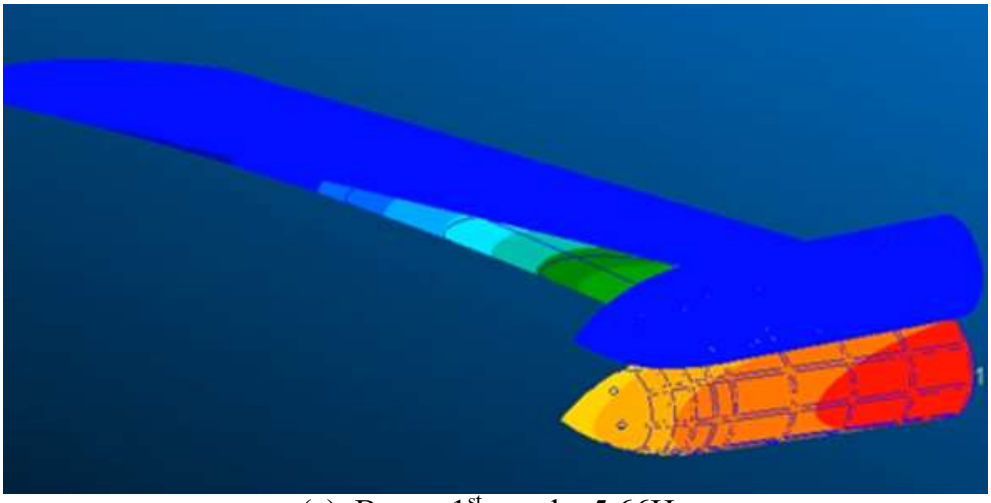

(a) Beam 1st mode 5.66Hz

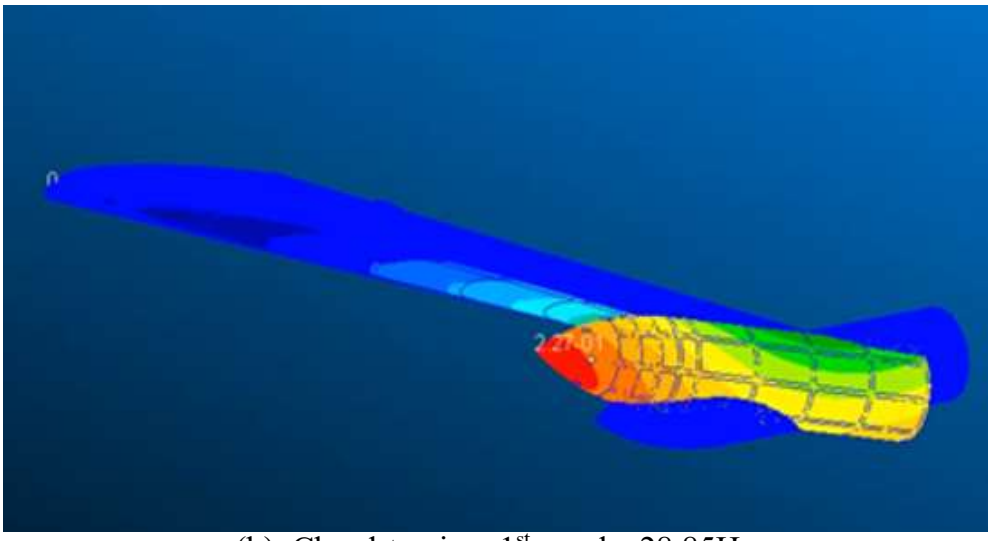

(b) Chord-torsion 1st mode 28.85Hz

Fig 3.6 Modal analysis result of Configuration 2 (contd.)

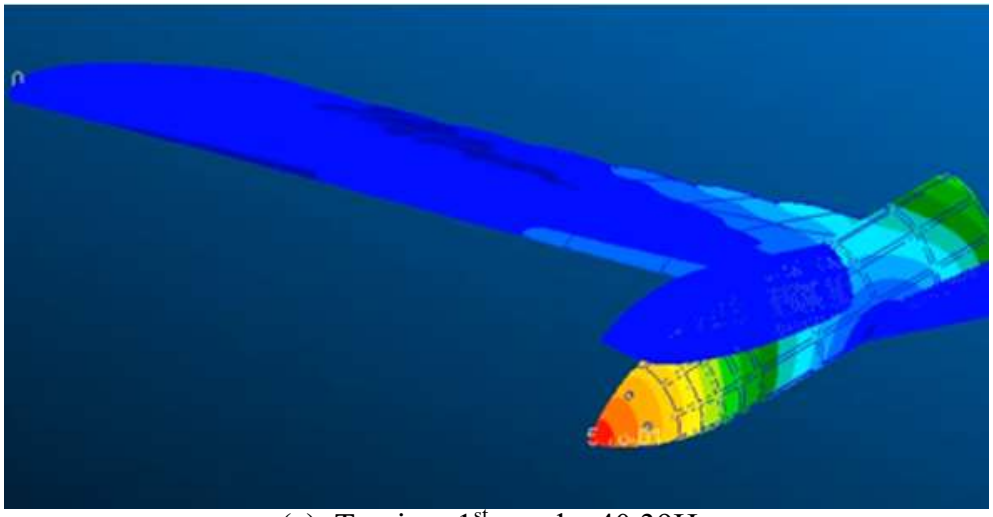

(c) Torsion 1st mode 40.39Hz

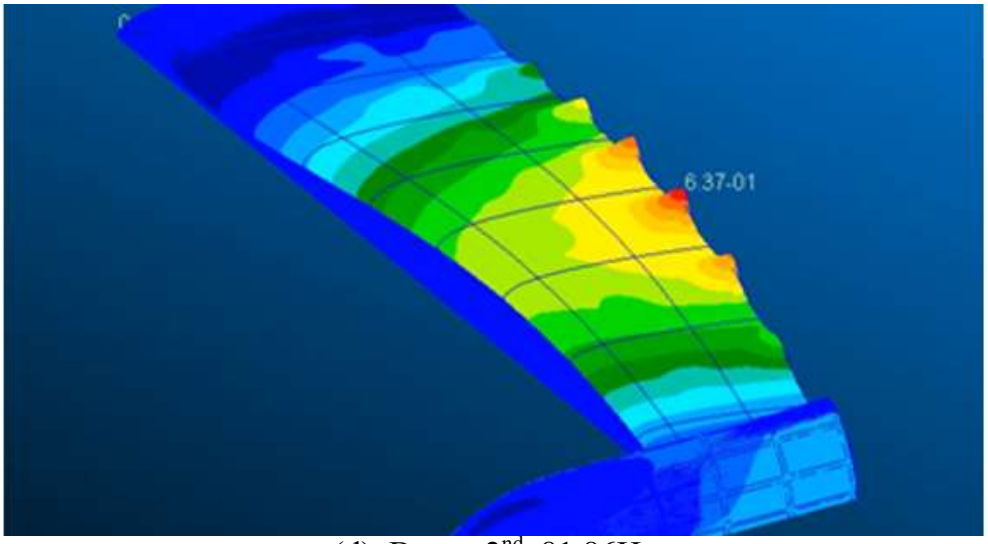

(d) Beam 2nd 81.86Hz

Fig 3.6 Modal analysis result of Configuration 2

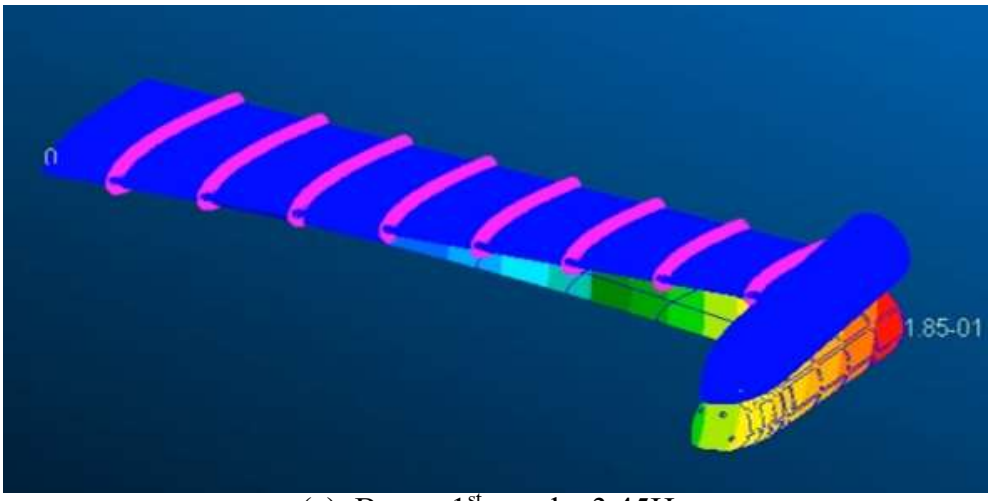

(a) Beam 1st mode 3.45Hz

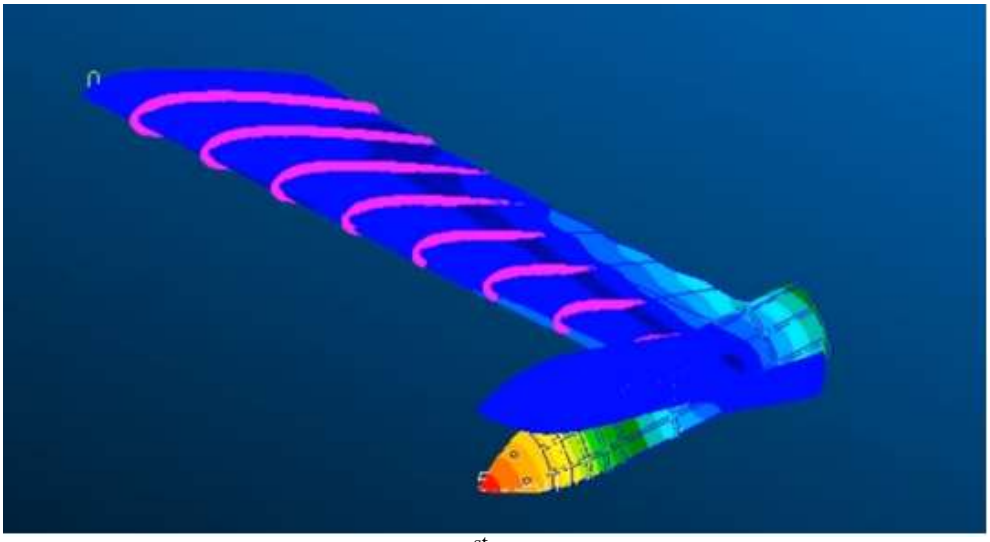

(b) Torsion 1st mode 16.01Hz

Fig 3.7 Modal analysis result of Configuration 3 (contd.)

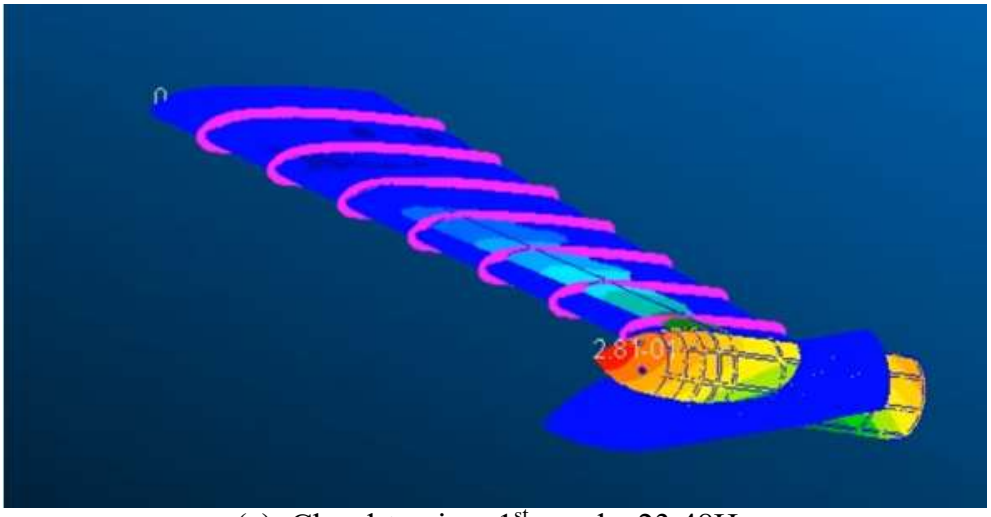

(c) Chord-torsion 1st mode 23.48Hz

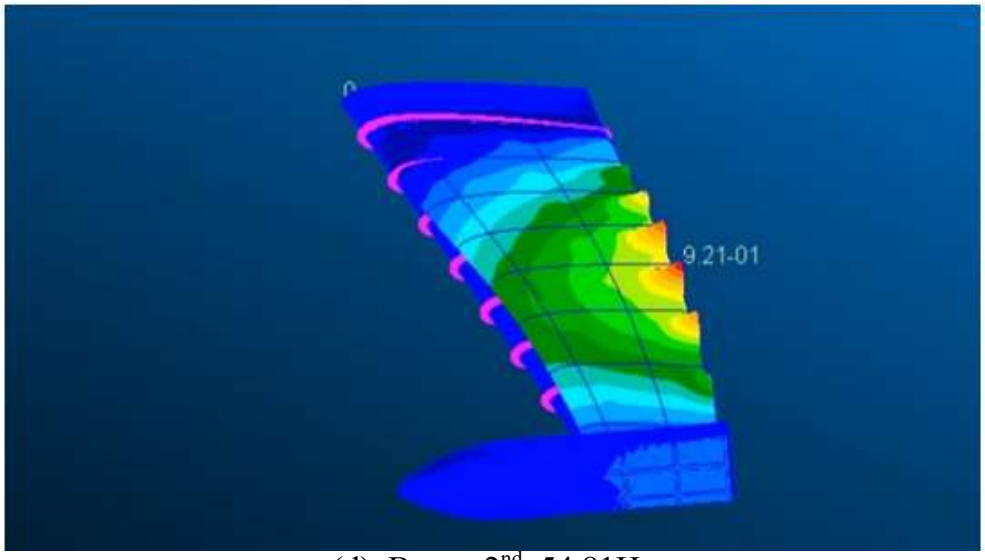

(d) Beam 2nd 54.81Hz

Fig 3.7 Modal analysis result of Configuration 3

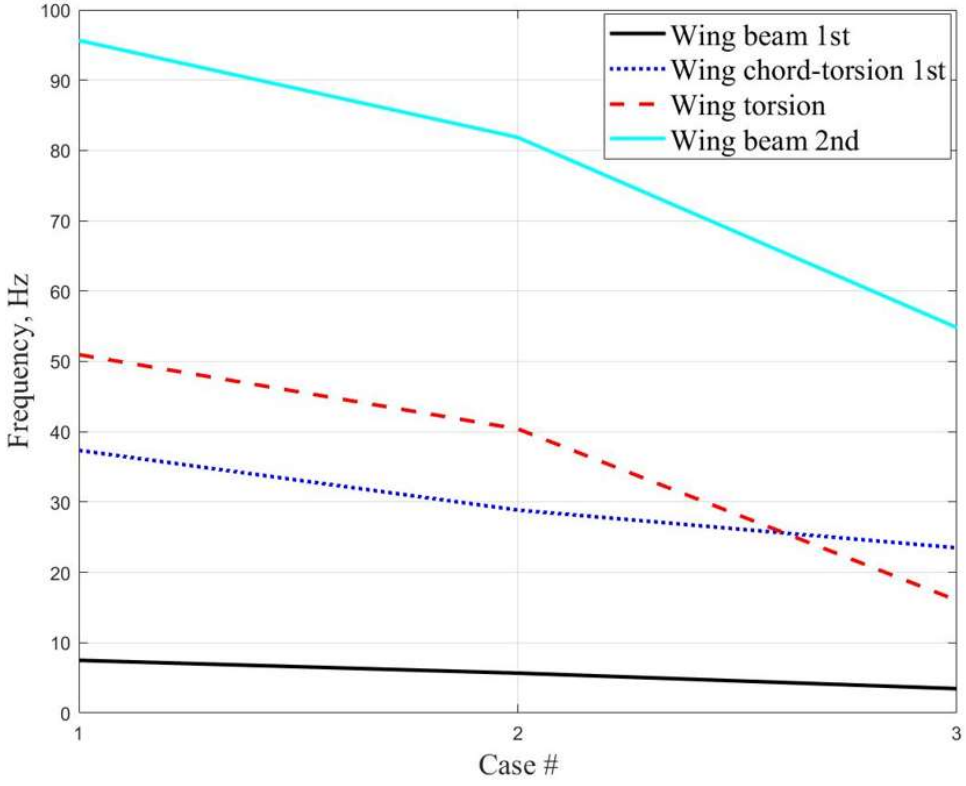

Fig 3.8 Modal analysis result comparison

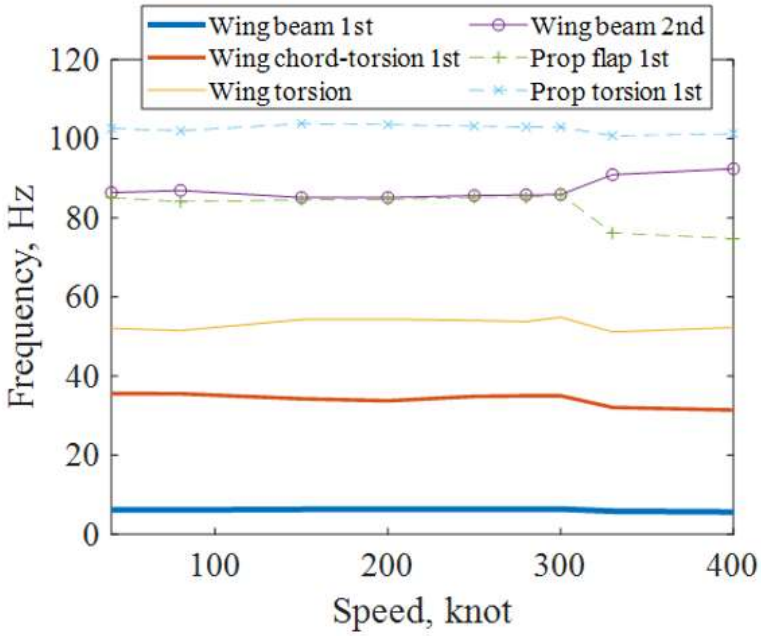

(a) Frequency vs speed

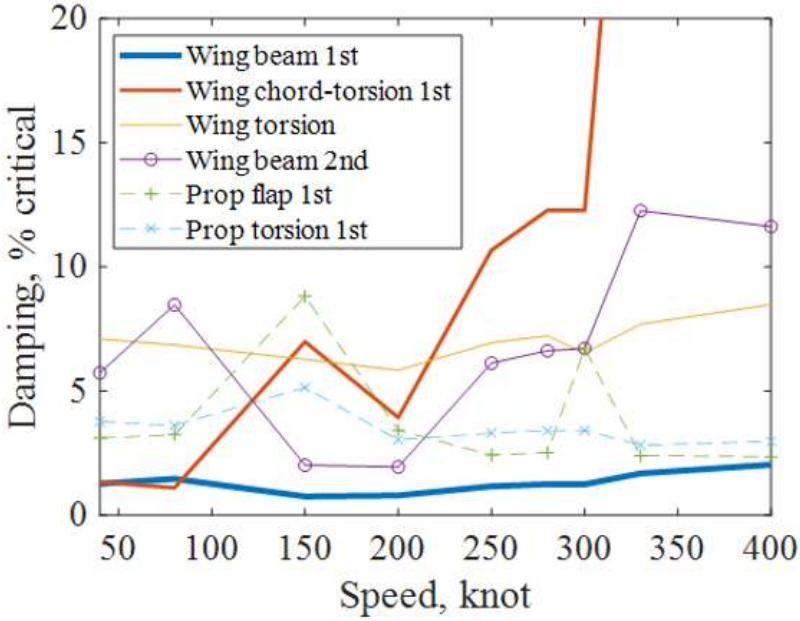

(b) Damping vs speed

Fig 3.9 Whirl flutter analysis result for Configuration 1 δ_3=-15º

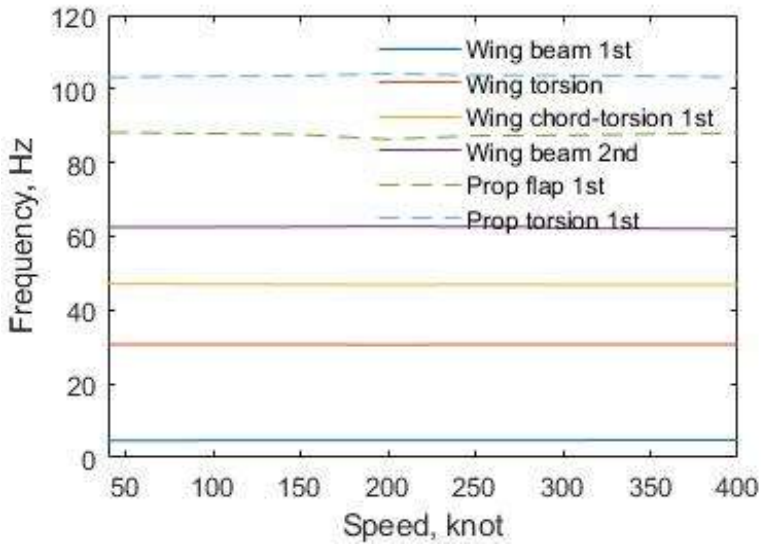

(a) Frequency vs speed

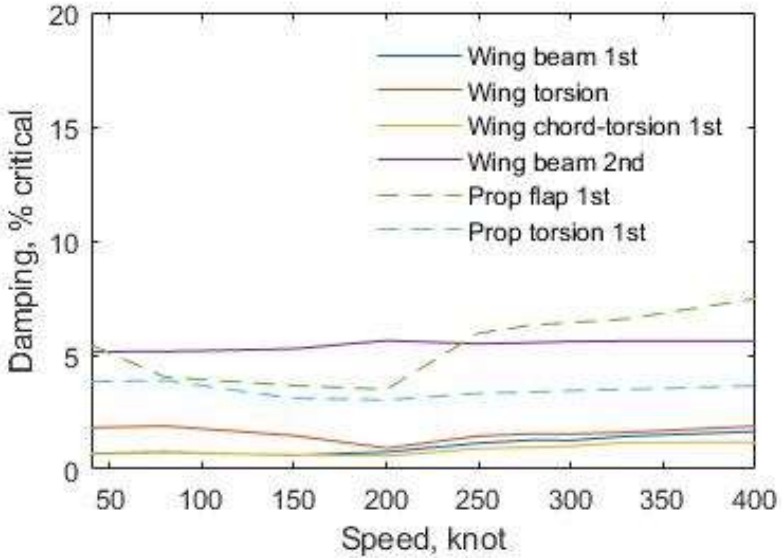

(b) Damping vs speed

Fig 3.10 Whirl flutter analysis result for Configuration 1 δ_3=-45º

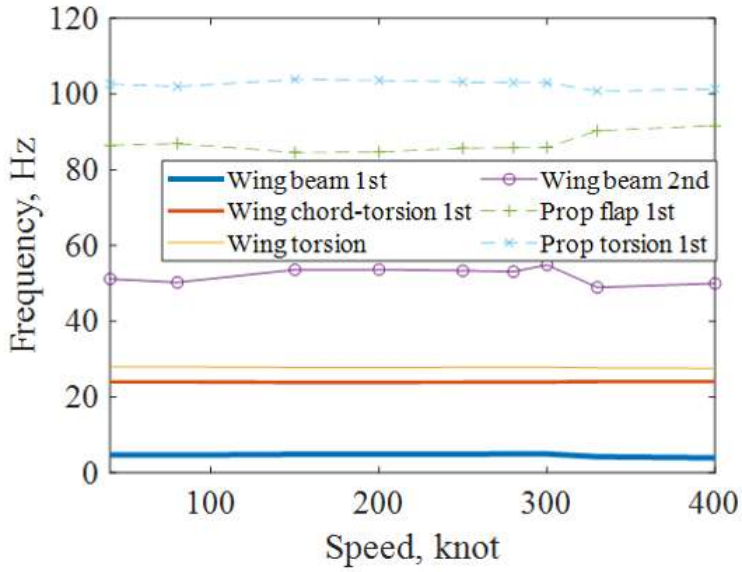

(a) Frequency vs speed

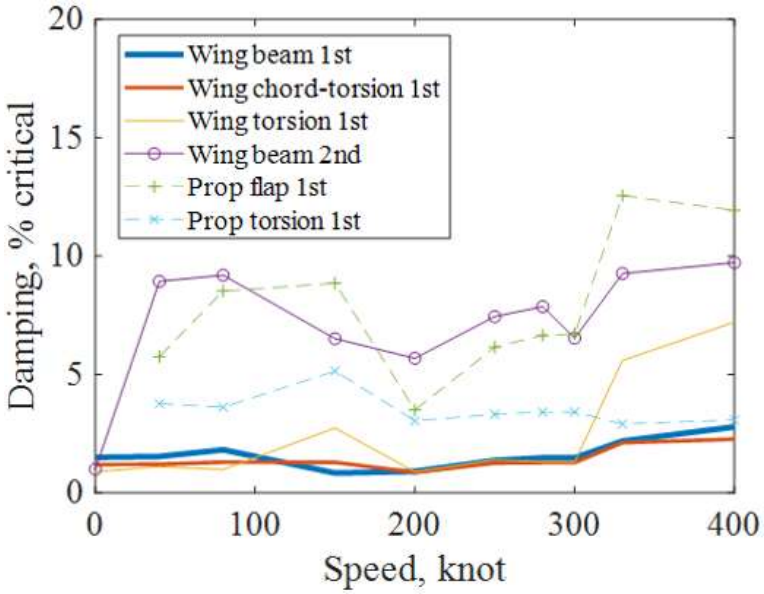

(b) Damping vs speed

Fig 3.11 Whirl flutter analysis result for Configuration 2 δ_3=-15º

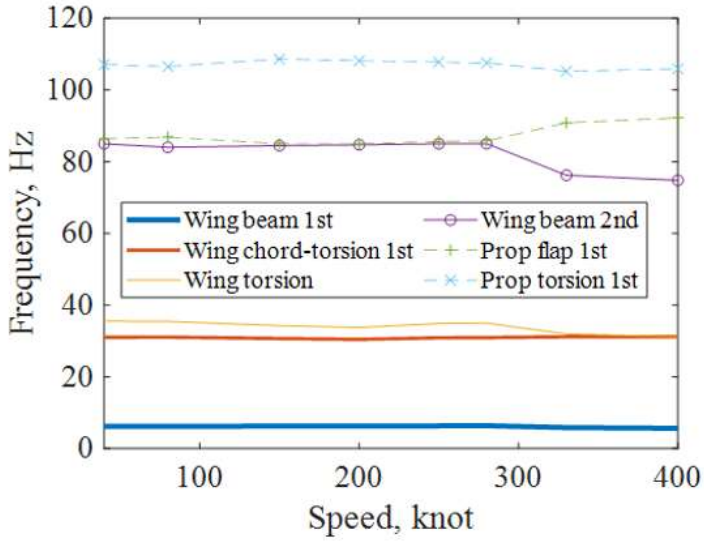

(a) Frequency vs speed

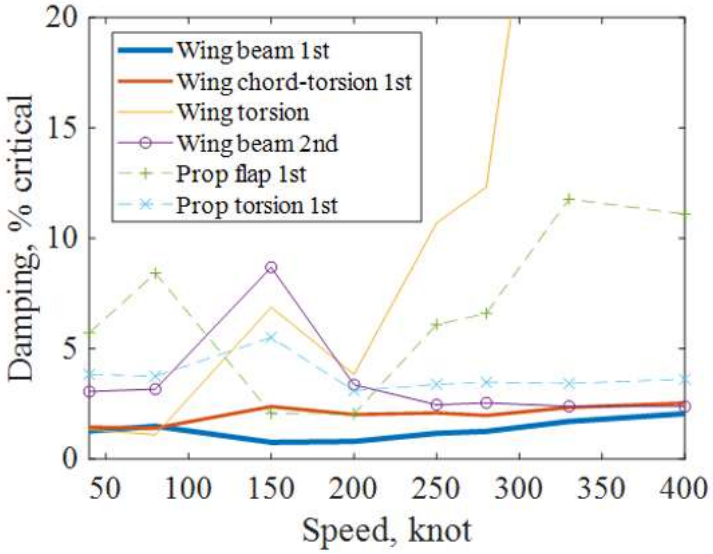

(b) Damping vs speed

Fig 3.12 Whirl flutter analysis result for Configuration 2 δ_3=-45º

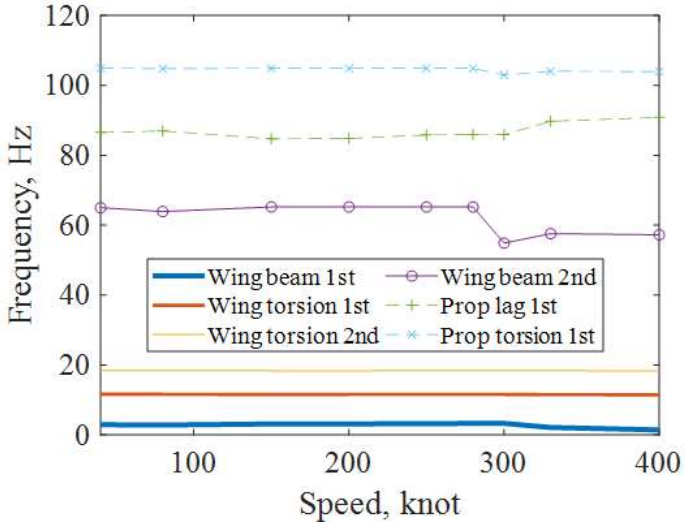

(a) Frequency vs speed

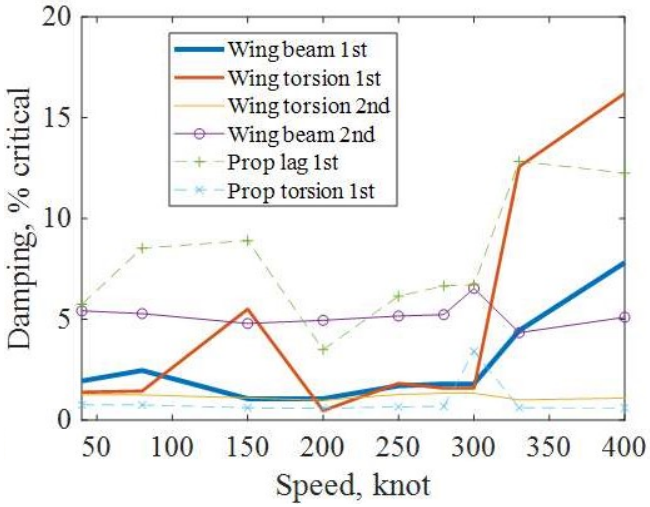

(b) Damping vs speed

Fig 3.13 Whirl flutter analysis result for Configuration 3 δ_3=-15º

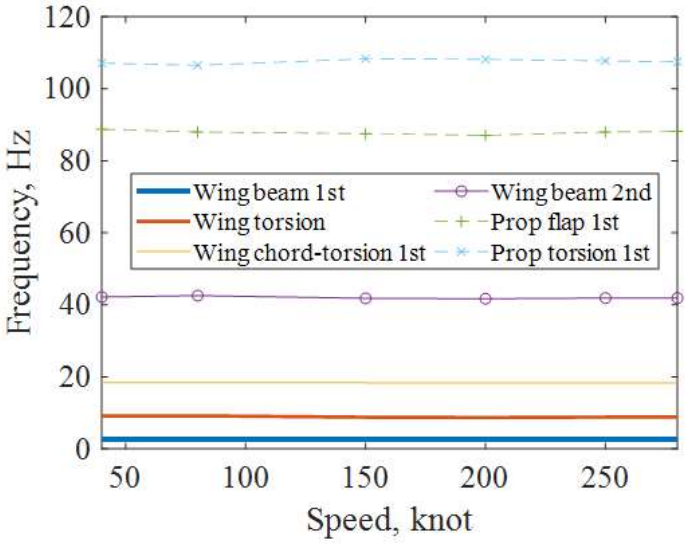

(a) Frequency vs speed

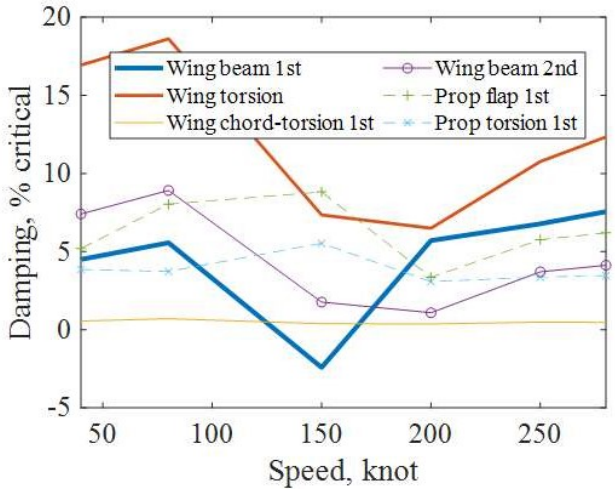

(b) Damping vs speed

Fig 3.14 Whirl flutter analysis result for Configuration 3 δ_3=-45º

Table 3.1 Modal analyses results

	1st mode (Hz)	2nd mode (Hz)	3rd mode (Hz)	4th mode (Hz)	5th mode (Hz)	6th mode (Hz)
Baseline (Configuration 1)	5.6	32.1	40.4	73.3	164.1	224.4
Configuration 4	5.3	30.6	38.3	71.7	160.0	217.8
Configuration 5	5.3	29.5	37.8	72.1	160.7	219.6
Configuration 6	4.8	29.2	36.6	67.7	152.5	208.4
Configuration 7	5.5	31.8	39.9	73.2	163.3	222.1
Configuration 8	5.6	31.6	39.8	73.2	163.0	222.5
Configuration 9	5.6	31.9	40.2	73.1	163.5	223.9
Configuration 10	5.6	31.3	39.9	72.5	161.9	223.1
Configuration 11	5.6	32.6	40.8	73.5	164.6	224.2

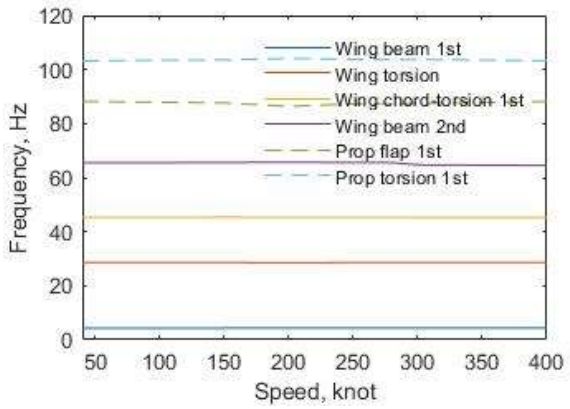

(a) Frequency vs speed

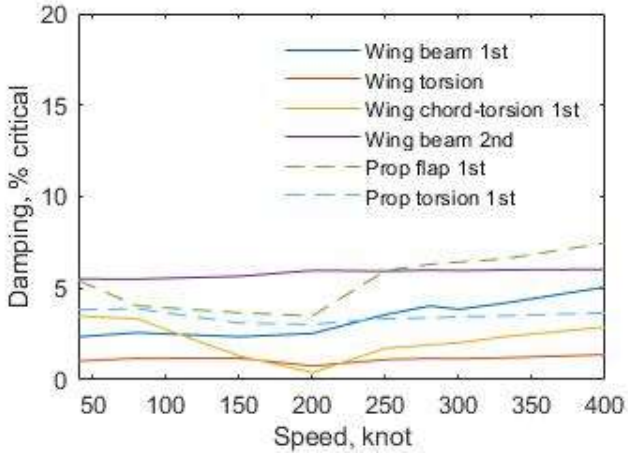

(b) Damping vs speed

Fig 3.15 Whirl flutter analysis result for Configuration 4

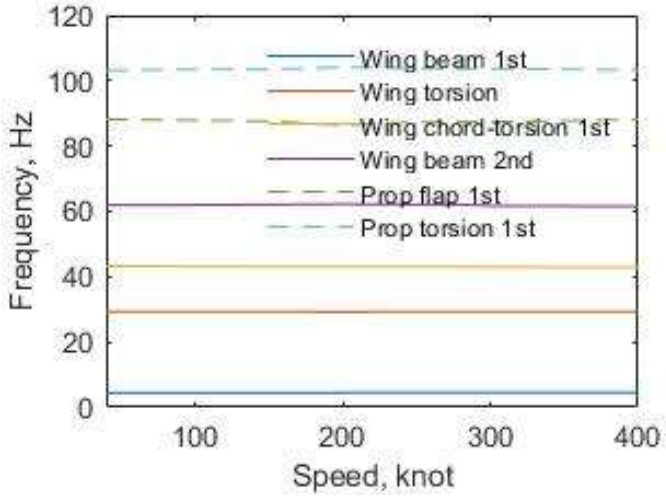

(a) Frequency vs speed

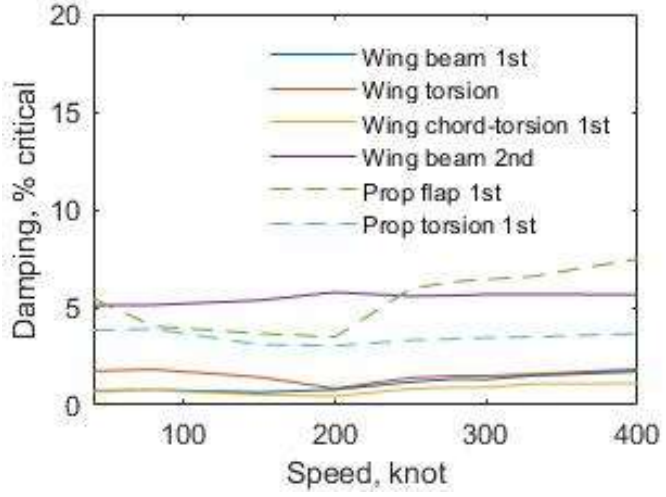

(b) Damping vs speed

Fig 3.16 Whirl flutter analysis result for Configuration 5

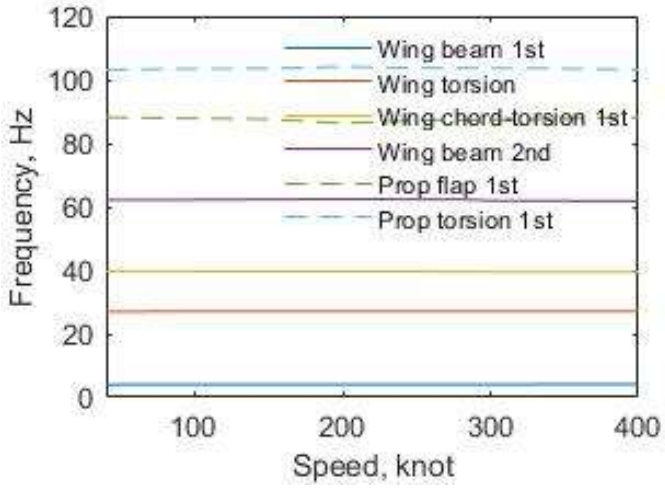

(a) Frequency vs speed

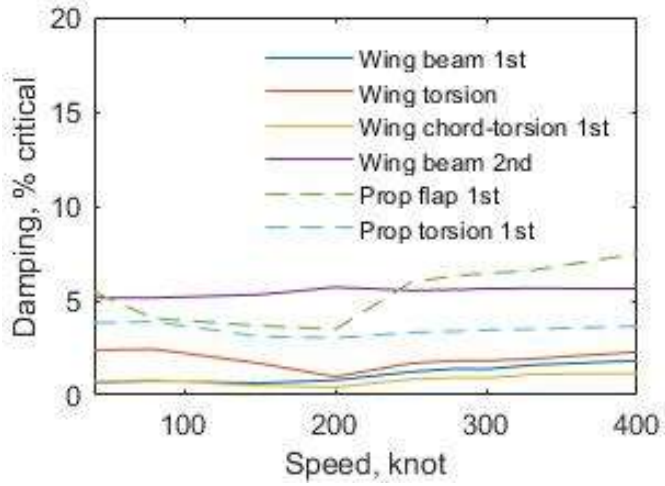

(b) Damping vs speed

Fig 3.17 Whirl flutter analysis result for Configuration 6

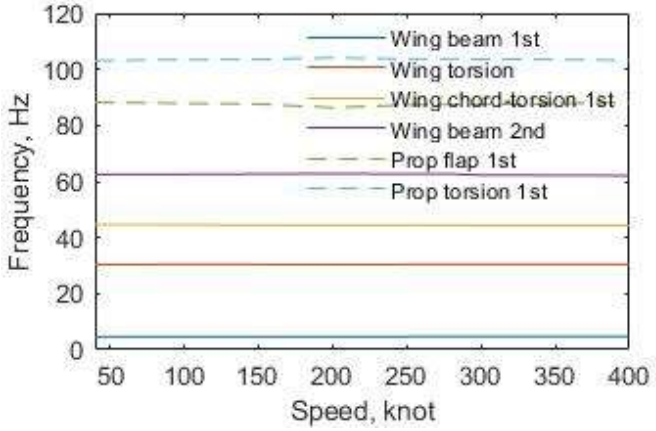

(a) Frequency vs speed

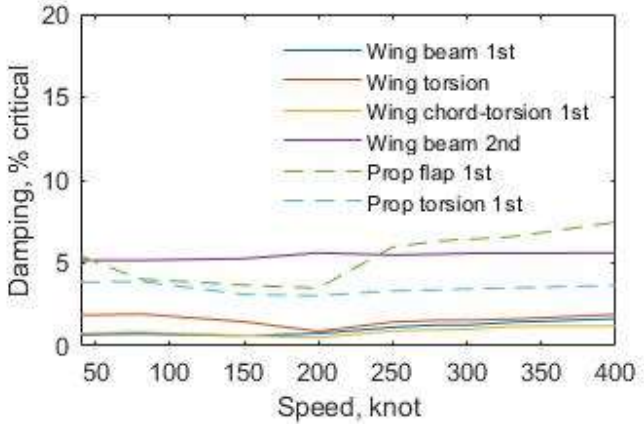

(b) Damping vs speed

Fig 3.18 Whirl flutter analysis result for Configuration 7

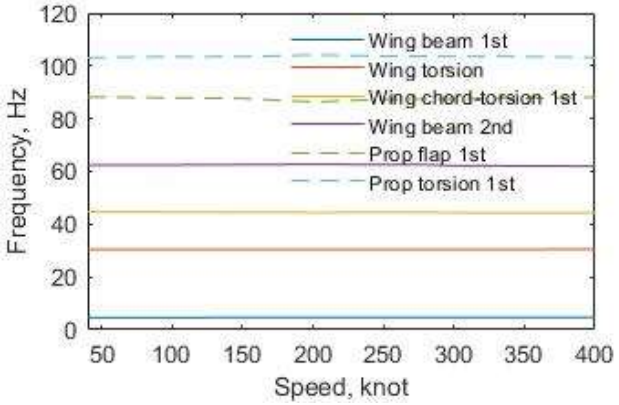

(a) Frequency vs speed

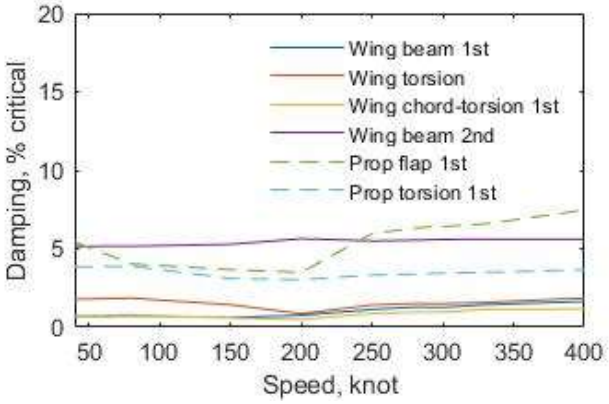

(b) Damping vs speed

Fig 3.19 Whirl flutter analysis result for Configuration 8

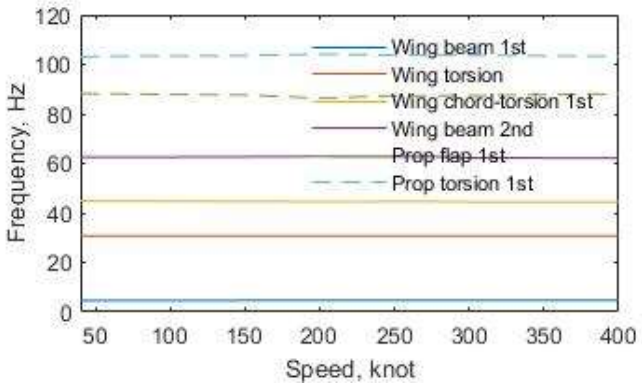

(a) Frequency vs speed

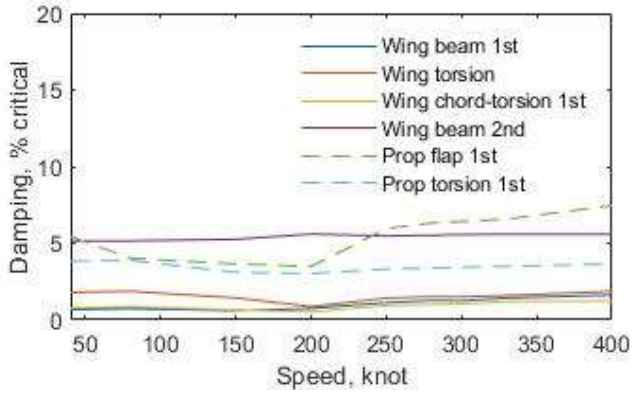

(b) Damping vs speed

Fig 3.20 Whirl flutter analysis result for Configuration 9

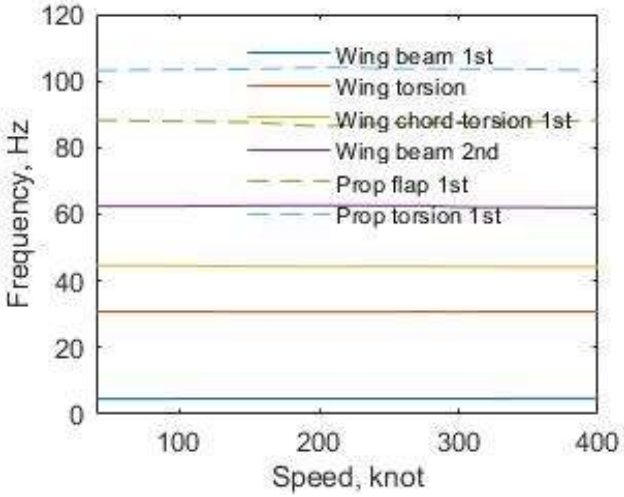

(a) Frequency vs speed

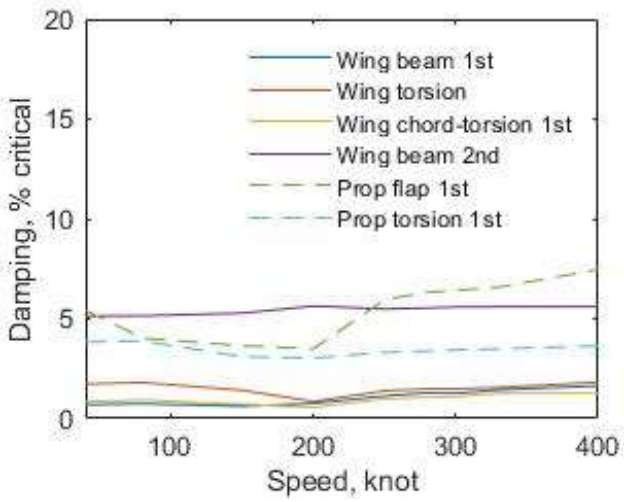

(b) Damping vs speed

Fig 3.21 Whirl flutter analysis result for Configuration 10

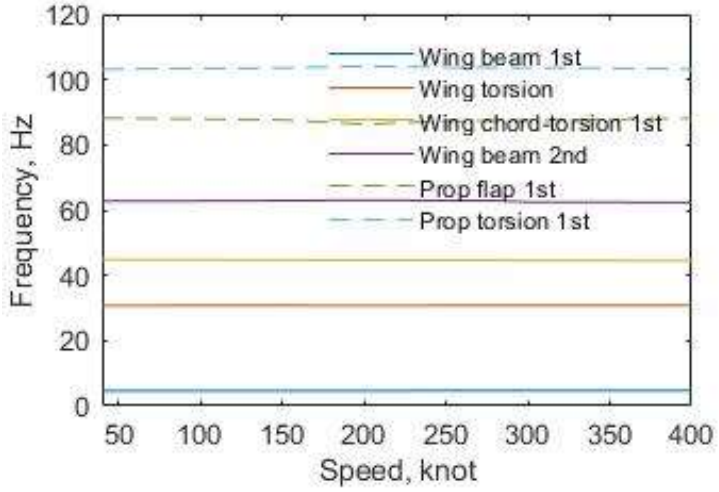

(a) Frequency vs speed

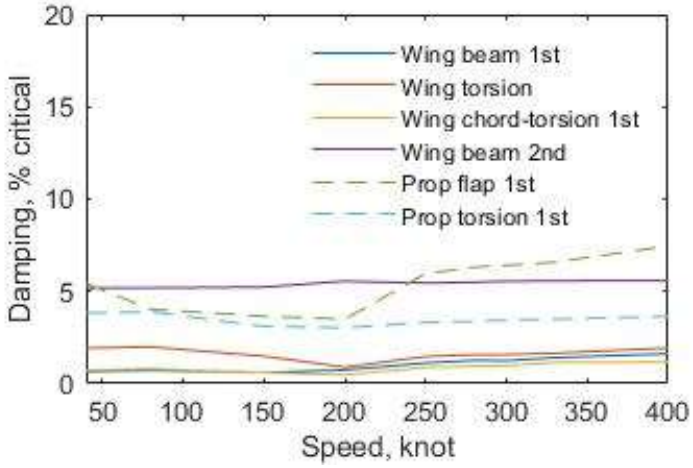

(b) Damping vs speed

Fig 3.22 Whirl flutter analysis result for Configuration 11

Table 3.2 The minimum critical damping and the total weight

	Minimum critical damping	The total weight(kg)
Baseline (Configuration 1)	5.8×10^{-3}	53.31
Configuration 4	4.0×10^{-3}	52.4
Configuration 5	4.5×10^{-3}	52.4
Configuration 6	4.2×10^{-3}	52.08
Configuration 7	5.0×10^{-3}	53.1
Configuration 8	4.8×10^{-3}	53.1
Configuration 9	5.2×10^{-3}	53.27
Configuration 10	5.6×10^{-3}	53.27
Configuration 11	4.8×10^{-3}	53.26

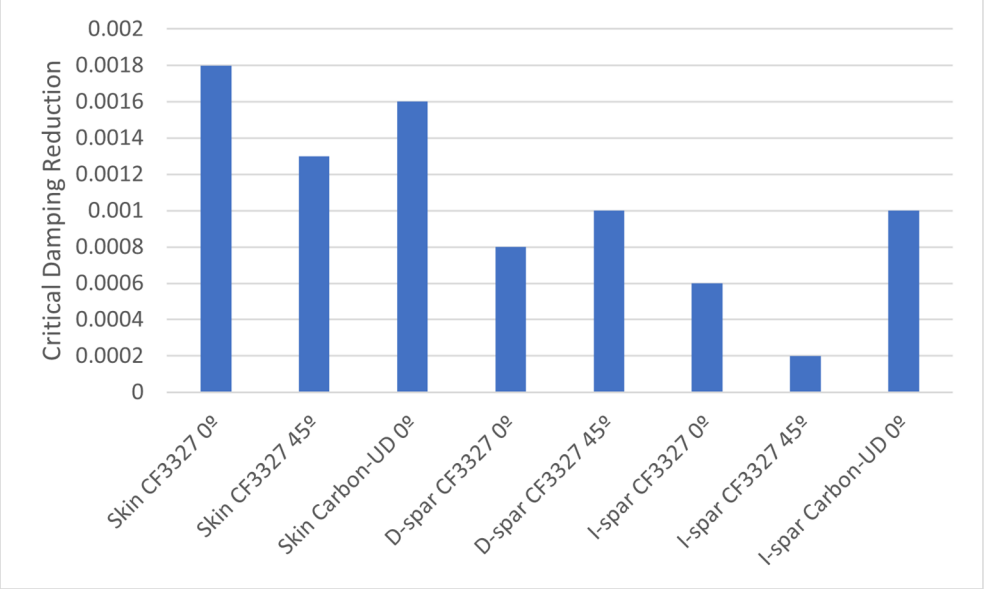

Fig 3.23 The critical damping value reduction tendency

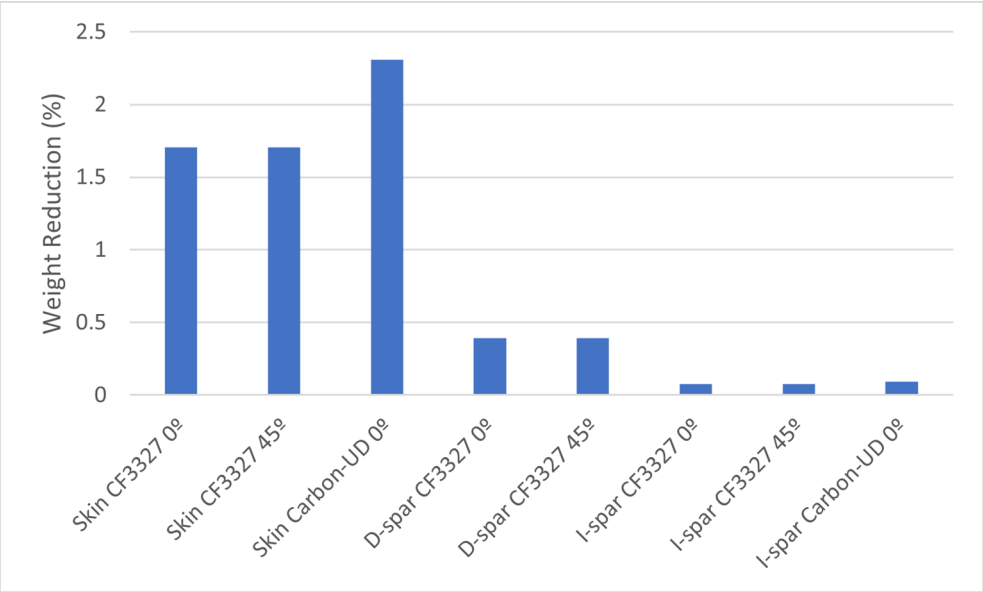

Fig 3.24 The weight reduction tendency

Chapter 4. Conclusion and Future Works

4.1 Conclusion

In this thesis, the wing for co-axial compound rotorcraft is designed and modal and whirl flutter analysis are performed. The wing has a prop-rotor nacelle on its tip, and thus the whirl flutter instability is one of the major concerns. Therefore, whirl flutter stability and static analysis are performed in this thesis. There are 3 composite materials applied to the components: GF108, CF3327, Carbon UD. 250kts cruising conditions are applied. For the design configurations, three different thickness configurations are considered. After the static and modal analysis are completed, the whirl flutter analyses are performed based on the mode frequencies and the eigenvectors from the modal analysis result. From the static analysis results, all configurations show enough safety margin by showing the maximum stress of the 60% of its allowable stress in the leanest configuration. However, in the whirl flutter stability analysis, most of the configurations show stable results. But the lightest configuration with -45^{o} of pitch-flap coupling shows unstable at the speed of 150kts. This is because the damping of the unstable modes varies almost linearly with the pitch-flap coupling and the reduction in the composite layer decrease the stiffness of the wing. Thus, a smaller magnitude of the pitch-flap coupling will be required to have enough stability margin for whirl flutter. Also, finding the minimum thickness with enough margin of safety will be important as

much as reducing the wing weight. In the trend analysis, it is shown that the same material may affect critical damping differently in terms of the different angle. This is because the stiffness in each direction can be varied with the angle of the plies and the damping toward a certain direction mode also. These analysis results can be utilized in constructing the design space for optimization.

4.2 Recommendation for Future Works

The following two items are recommended for future development.

1. The trend analysis with the other design parameters will need to be conducted. With such trend analyses, important design parameters will be chosen and the sensitivity analysis will be performed. Proper sensitivity analysis will be required to perform an optimization.
2. Investigation on the various configuration of the rotor will be needed. As shown in this thesis, the pitch-flap coupling affects the whirl flutter stability, but the angle can be varied with regard to what type of rotor is utilized. The rotor with a smaller pitch-flap coupling can bring enhanced stability margin for whirl flutter by adopting a lighter wing.

References

[1] Leishman, J.G., “Principles of Helicopters Aerodynamics,” Cambridge University Press, Cambridge, NY, 2006

[2] Berger, T., Ott, C., Cox, J., Cecchis, P.D., Wood, J., “Flight Test Assessment of the Break Turn and High-Speed Acceleration / Deceleration Mission Task Elements using a UH-60M Black Hawk,” Vertical Flight Society 75th Annual Forum, 2019.

[3] Lee, D.W., Jeong, S,M., and Yee, K.J., “Development of a Conceptual Design Tool for Various Compound Helicopters,” 44th European Rotorcraft Forum, 2018.

[4] Chun, T.Y., Park, S.H. and Shin, S.J., “Trade-off Design Study on a High Speed Fan-in-Wing Rotorcraft using Optimization,” Proceedings of 7th Asian/Australian Rotorcraft Forum, 2018.

[5] Yeo, H. and Johnson, W., “Optimum Design of a Compound Helicopter,” Journal of Aircraft, 46(4), 2009, pp.1210~1221.

[6] Lim, J. H., Shin, S. J., Kee, Y. J., “Optimization of Rotor Structural Design in Compound Rotorcraft with Lift Offset,” Journal of the American Helicopter Society, 61(1), 2016, pp.1-14.

[7] Hersey, S., Sridharan, A. and Celi, R., “Multiobjective Performance Optimization of a Coaxial Compound Rotorcraft Configuration,” Journal of Aircraft, 54(4), 2017, pp.1498~1507.

[8] Shen, J., Kang, H., “Comparison Study of Tiltrotor Whirl Flutter Using Two Rotorcraft Comprehensive Analyses,” Journal of Aircraft, 54(2), 2017, pp.841~846.

[9] Yeo, H., Bosworth, J., Acree Jr., C. W., and Kreshock, A. R., “Comparison of CAMRAD II and RCAS Predictions of Tiltrotor Aeroelastic Stability,” Journal of the American Helicopter Society, 63(2),

2018, pp.1~pp.13

[10] Yeo, H., Kreshock, A. R., “Whirl Flutter Investigation of Hingeless Proprotors,” Journal of Aircraft, 57(4), 2020, pp.586~596.

[11] Henry, T. C., Riddick, J. C., Mills, B. T., Habtour, E. M., “Composite Driveshaft Prototype Design and Survivability Testing,” Journal of Composite Materials, 51(16), 2017, pp.2377~2386.

[12] Endres, M., “Experimental Study of Two Electro-mechanical De-icing Systems Applied on a Wing Section Tested in an Icing Wind Tunnel,” CEAS Aeronaut J, 8(3), 2017, pp.429~439.

[13] Dharmendra, P., “Design and Analysis of an Aircraft Wing Rib for Diffrent Configurations,” International Research Journal of Engineering and Technology, 7(6), 2020, pp.180~191.

[14] Cecrdle, J., “Aeroelastic Stability of Turboprop Aircraft: Whirl Flutter,” Flight Physics - Models, Techniques and Technologies, Intech, 2018.

[15] Yeo, H., Kang, H., and Kreshock, A. R., “Modeling and Analysis of Proprotor Whirl Flutter,” 77th Vertical Flight Society Forum, 2021

[16] Acree Jr., C. W., Peyran, R. J., and Johnson, W., “Rotor Design Options for Improving XV-15 Whirl-Flutter Stability Margins,” Journal of the American Helicopter Society, 46(2), 2001, pp.87~95.

국문 초록

휠 플러터 안정성을 고려한 동축 반전형 복합형 회전익기 주익의 설계 연구

염제완
서울대학교 대학원
협동과정 우주시스템전공

회전익기는 특유의 수직 이착륙과 제자리 비행 기능으로 다양한 분야에서 활용되어 왔으나, 압축성 효과, 공력탄성학적 안정성, 실속과 같은 이유로 최대 속도와 운용 반경에서 제약이 존재했다. 최근에는 기존 회전익기의 장점을 유지하면서 단점을 상쇄하고 고정익기의 장점을 동시에 보유한 복합형 회전익기에 대한 연구가 활발히 이루어지고 있다. 이러한 복합형 회전익기 중에는 주익에 프롭로터가 위치한 형상들도 존재하는데, 그러한 형상들의 경우 축류에 의해 프로펠러/나셀 시스템이 섭동되거나 짐발허브의 플래핑 자유도로 인해 세차운동을 하며 공력 하중이 발생하게 된다. 그리고 이러한 하중에 의해 휠플러터가 유발되므로 주익에 프롭로터가 위치한 복합형 회전익기는 설계 시 휠플러터가 고려되어야 한다. 본 논문에서는 동축반전형 복합형 회전익기의 3차원 형상을 설계하였다. 이후 3가지 형상을 제안하여, NASTRAN을 활용한 구조적 설계 여유와 CAMRAD II를 통한 휠플러터 해석을 수행하였으며 그 중 기본 형상을 정하고

이 형상에서 각 변수를 조절하며 임계 감쇠 값의 경향을 분석하였다.

주제어: 복합형 회전익기, 주익, 구조 해석, 휠플러터 해석
학번: 2019-29018